J|A|C|S
ARTICLES
Published on Web 03/06/2007

Continuum of Outer- and Inner-Sphere Mechanisms for Organic Electron Transfer. Steric Modulation of the Precursor Complex in Paramagnetic (Ion-Radical) Self-Exchanges

Sergiy V. Rosokha and Jay K. Kochi*

Contribution from the Department of Chemistry, University of Houston, Houston, Texas 77204

Received December 20, 2006; E-mail: jkochi@uh.edu

Abstract: Transient 1:1 precursor complexes for intermolecular self-exchange between various organic electron donors (**D**) and their paramagnetic cation radicals ($\mathbf{D}^{+\bullet}$), as well as between different electron acceptors (**A**) paired with their anion radicals ($\mathbf{A}^{-\bullet}$), are spectrally (UV−NIR) observed and structurally (X-ray) identified as the cofacial (π-stacked) associates [**D**, $\mathbf{D}^{+\bullet}$] and [$\mathbf{A}^{-\bullet}$, **A**], respectively. Mulliken−Hush (two-state) analysis of their diagnostic intervalence bands affords the electronic coupling elements (H_{DA}), which together with the Marcus reorganization energies (λ) from the NIR spectral data are confirmed by molecular-orbital computations. The H_{DA} values are found to be a sensitive function of the bulky substituents surrounding the redox centers. As a result, the steric modulation of the donor/acceptor separation (r_{DA}) leads to distinctive electron-transfer rates between sterically hindered donors/acceptors and their more open (unsubstituted) parents. The latter is discussed in the context of a continuous series of outer- and inner-sphere mechanisms for organic electron-transfer processes in a manner originally formulated by Taube and co-workers for inorganic (coordination) donor/acceptor dyads—with conciliatory attention paid to traditional organic versus inorganic concepts.

1. Introduction

H. Taube and co-workers[1] more than 50 years ago conceived electron-transfer processes of inorganic (coordination) compounds in terms of two distinctive mechanistic categories based on the nature of the rate-limiting transition states.[2,3] In *outer-sphere electron transfer*, the bimolecular transition state (TS) is traversed with the separate coordination spheres of both the electron donor (**D**) and the electron acceptor (**A**) essentially intact,[4] whereas, in the *inner-sphere mechanism*, the unimolecular (collapsed) transition state typically results from the mutual interpenetration of coordination spheres via a critical bridging ligand (L),[5] as schematically depicted in Chart 1 with $\mathbf{D} = \mathrm{M'L_6}^{+n}$ and $\mathbf{A} = \mathrm{ML_6}^{+n+1}$ representing a pair of octahedral complexes.[6]

The phenomenological kinetics of outer- and inner-sphere electron transfers share a common pathway involving three basic transformations: (a) the diffusive association of the donor/acceptor pair to form the 1:1 precursor complex [**D,A**] followed by (b) the rate-limiting intracomplex electron transfer to afford the successor complex [$\mathbf{D}^{+\bullet}$,$\mathbf{A}^{-\bullet}$], and then (c) the diffusive separation that is (more or less) akin to step (a) in microscopic reverse. However, these rate processes are strongly divergent when the electronic coupling element for the precursor complex is quantitatively taken into account, with $H_{DA} \lesssim 200\ \mathrm{cm}^{-1}$ for the outer-sphere pathway[7] and substantially greater values pertaining to inner-sphere electron transfer.[8,9]

From a purely conceptual point of view, the outer-sphere pathway is relatively more readily managed theoretically since Marcus[10] demonstrated how the electron-transfer rates can be

Chart 1

(1) (a) Taube, H.; Myers, H. *J. Am. Chem. Soc.* **1954**, *76*, 2103. (b) Taube, H.; Myers, H. J.; Rich, R. L. *J. Am. Chem. Soc.* **1953**, *75*, 4118. (c) Taube, H. Nobel Lecture: *Angew. Chem., Int. Ed. Engl.* **1984**, *23*, 329.
(2) (a) Taube, H. *Adv. Inorg. Radiochem.* **1959**, *1*, 1. (b) Taube, H. *Electron-Transfer Reactions of Complex Ions in Solution;* Academic: New York, 1970. (c) Meyer, T. J.; Taube, H. In *Comprehensive Coordination Chemistry*; Wilkinson, G., Guilard, R., McLafferty, J. A., Eds.; Pergamon: London, 1987; p 331 ff.
(3) For example, also see: (a) Lippard, S. J. *Prog. Inorg. Chem.* **1983**, *30*, 1. (b) Cannon, R. D. *Electron Transfer Reactions*; Butterworth: London, 1980. (c) Astruc, D. *Electron Transfer and Radical Processes in Transition-Metal Chemistry*; VCH: New York, 1995.
(4) For example, see: Reynolds, W. L.; Lumry, R. W. *Mechanism of Electron Transfer*; Ronald Press: New York, 1966.
(5) (a) Haim, A. *Prog. Inorg. Chem.* **1983**, *30*, 273. (b) Haim, A. *Acc. Chem. Res.* **1975**, *8*, 264. (c) Schwarz, C. L.; Endicott, J. F. *Inorg. Chem.* **1995**, *34*, 4572.
(6) (a) Generally speaking, a separate deligation step will precede the formation of the bridged-activated complex unless the donor or acceptor is coordinatively unsaturated. (b) In Taube and Myers' original study,[1] the rapid loss of an aquo ligand from the substitution-labile chromium(II) donor occurs prior to the formation of the chloro-bridged precursor (activated) complex with the chlorocobalt(III) acceptor.
(7) (a) Logan, J.; Newton, M. D. *J. Chem. Phys.* **1983**, *78*, 4086. (b) Rosso, K. M.; Smith, D. M.; Dupuis, M. *J. Phys. Chem. A* **2004**, *108*, 5242.
(8) Compare the evaluation of H_{DA} in various $\mathrm{Ru^{II}}$(bridge)$\mathrm{Ru^{III}}$ systems: (a) Creutz, C.; Taube, H. *J. Am. Chem. Soc.* **1969**, *91*, 3988. (b) Creutz, C. *Prog. Inorg. Chem.* **1983**, *30*, 1.
(9) See also: (a) Demadis, K. D.; Hartshorn, C. M.; Meyer, T. J. *Chem. Rev.* **2001**, *101*, 2655. (b) Evans, C. E. B.; Naklicki, M. L.; Rezvani, A. R.; White, C. A.; Kondratiev, V. V.; Crutchley, R. J. *J. Am. Chem. Soc.* **1998**, *120*, 13096.

10.1021/ja069149m CCC: $37.00

predicted from the structural properties of the individual (intact) donor and acceptor. However, the comparable simplicity cannot be so easily invoked for the inner-sphere activated complex, and the calculations of the inner-sphere electron-transfer rates have been significantly more difficult, with one exception involving the isolable donor−bridge−acceptor or mixed-valence complex.[8,9] Thus Hush[11] and Sutin[12] showed how the characteristic intervalence (IV) absorption bands extant with various donor/acceptor dyads can be applied to the evaluation of the critical electronic coupling element (H_{DA}) in the corresponding mixed-valence complex for intramolecular electron transfer. However, the evaluation of H_{DA} for *intermolecular* electron transfer can be complicated by slow (intervening) ligand substitutions[6] required for octahedral structures (see Chart 1).[13] Notably, such rate-limiting steps are avoided entirely in inner-sphere electron transfer with many organic donor/acceptor dyads in which direct electronic coupling of the redox centers can occur without "ligand" involvment.[14,15] Therefore at this juncture, let us bifurcate our brief historical summary and exclude the outer-sphere pathway from further detailed consideration because it has already been successfully dealt with in extended scope, breadth, and prolonged depth.[3,4,16,17] By way of contrast, there are almost no quantitative studies of inner-sphere electron transfer, which we simply attribute to the dearth of experimental data on the nature of the inner-sphere (strongly adiabatic) transition state for intermolecular electron transfer.[18] Indeed, the latter is again understandable in a historical context because quantitative studies of electron-transfer processes have heretofore largely focused on inorganic octahedral (and related high-coordination) complexes that do not particularly favor close donor/acceptor encounters, largely for symmetry/steric reasons.[14] When Mulliken[19,20] first considered the intermolecular potentials of diffusive interactions, he showed that many types of organic (and main-group metal) donor/acceptor dyads easily form a wide variety of intermolecular [1:1] complexes that can be readily monitored quantitatively via their characteristic charge-transfer (CT) absorption bands.[20,21]

Accordingly, we now focus on inner-sphere electron transfer in two distinctly separate but strongly related classes of organic donor/acceptor dyads. Here in Part 1, we quantitatively examine the fast kinetics and (isergonic) energetics of electron-transfer *self-exchange* (SE) specifically between planar π-donors (**D**) and their oxidized cation radicals ($\mathbf{D}^{+\bullet}$), as well as between planar π-acceptors (**A**) and their reduced anion radicals ($\mathbf{A}^{-\bullet}$), i.e.,

$$\mathbf{D} + \mathbf{D}^{+\bullet} \overset{k_{SE}}{\rightleftharpoons} \mathbf{D}^{+\bullet} + \mathbf{D} \quad (1a)$$

$$\mathbf{A}^{-\bullet} + \mathbf{A} \overset{k_{SE}}{\rightleftharpoons} \mathbf{A} + \mathbf{A}^{-\bullet} \quad (1b)$$

In eq 1, the paramagnetic 1:1 associates [$\mathbf{D},\mathbf{D}^{+\bullet}$] and [$\mathbf{A}^{-\bullet},\mathbf{A}$], respectively, would represent the donor/acceptor precursor complex relevant to the self-exchange process.[22,23] As such, the spectral observation and scrutiny of the Hush intervalence absorption band together with the isolation and X-ray analysis of [$\mathbf{D},\mathbf{D}^{+\bullet}$] and [$\mathbf{A}^{-\bullet},\mathbf{A}$] will then form the critical facet in the inner-sphere electron-transfer pathway.[24−28] In Part II,[29] we enlarge the structural diversity to encompass different organic functionalities in electron-transfer *cross-exchange* as allowed by Mulliken charge-transfer theory[19−21] for diamagnetic (uncharged) donor/acceptor dyads, i.e.,

$$\mathbf{D} + \mathbf{A} \overset{k_{CE}}{\rightleftharpoons} \mathbf{D}^{+\bullet} + \mathbf{A}^{-\bullet} \quad (2)$$

2. Results

The prime requirement for the quantitative analysis of organic self-exchange dynamics is the availability of crystallographically (X-ray) well-defined salts of the ion-radicals $\mathbf{D}^{+\bullet}$ and $\mathbf{A}^{-\bullet}$ so that their kinetic behavior is relatively unaffected by their counterions when these pure salts are dissolved in aprotic organic solvents to minimize (strong) solvation effects. Accordingly, all the cation radicals for eq 1a (Table 1) were

(10) (a) Marcus, R. A. *Discuss. Faraday Soc.* **1960**, *29*, 21. (b) Marcus, R. A. *J. Phys. Chem.* **1963**, *67*, 853. (c) Marcus, R. A. *J. Chem. Phys.* **1965**, *43*, 679. (d) Marcus, R. A. *Rev. Mod. Phys.* **1993**, *65*, 599. (e) Marcus, R. A.; Sutin, N. *Biochim. Biophys. Acta* **1985**, 811, 265.
(11) Hush, N. S. *Prog. Inorg. Chem.* **1967**, *8*, 391.
(12) Sutin, N. *Prog. Inorg. Chem.* **1983**, *30*, 441.
(13) (a) The vast majority of quantitative electron-transfer studies of inorganic coordination compounds have been carried out with octahedral complexes, especially when compared to those with a lower metal coordination number, such as linear, square planar, square pyramidal, etc. For the necessity of the separate substitution step, see: Kochi, J. K.; Powers, J. W. *J. Am. Chem. Soc.* **1970**, *92*, 137. (b) We anticipate that inorganic electron-transfer reactions with coordinatively unsaturated metal (coordination) donors and acceptors with square planar coordination, etc., will reveal intermolecular charge-transfer bands. (c) See: Kochi, J. K. *Angew. Chem., Int. Ed. Engl.* **1988**, *27*, 1227.
(14) (a) The best organic electron donors and acceptors are generally substitution-stable and contain planar (aromatic and olefinic) redox centers that are sterically favorable for intermolecular π-interactions. (b) By comparison, intermolecular interactions are less favorable with quasi-spherical (octahedral) systems. For example, see: (b) Veya, P.; Kochi, J. K. *J. Organomet. Chem.* **1995**, *488*, C4. (c) Le Magueres, P.; Hubig, S. M.; Lindeman, S. V.; Veya, P.; Kochi, J. K. *J. Am. Chem. Soc.* **2000**, *122*, 10073. (d) Masnovi, J. M.; Huffman, J. C.; Kochi, J. K. Hilinski, E. F.; Rentzepis, P. M. *Chem. Phys. Lett.* **1984**, *106*, 20.
(15) (a) Mulliken, R. S. *J. Am. Chem. Soc.* **1952**, *74*, 811. (b) Kochi, J. K. *Comprehensive Organic Synthesis*; Trost, B. M., Fleming, I., Ley, S. V., Eds.; Pergamon: New York, 1991; Vol. 7, p 849ff. (c) Rathore, R.; Kochi, J. K. *Adv. Phys. Org. Chem.* **2000**, *35*, 193. (d) The earlier monograph by Eberson, L. entitled: *Electron Transfer in Organic Chemistry* (Springer: London, 1987) is unnecessarily restrictive because all redox processes are uniformly (and unjustifiably) treated by the classical Marcus (outer-sphere) formalism.
(16) (a) Marcus, R. A. *Angew. Chem., Int. Ed. Engl.* **1993**, *32*, 1111. (b) Chou, M.; Creutz, C.; Sutin, N. *J. Am. Chem. Soc.* **1977**, *99*, 5615. (c) Bixon, M.; Jortner, J. *Adv. Chem. Phys.* **1999**, *106*, 35.
(17) (a) Gray, H. B.; Winkler, J. R. In *Electron Transfer in Chemistry, Vol. III: Biological Systems*; Balzani, V., Ed.; Wiley-VCH: New York, 2001. (b) Piotrowiak, P. In *Electron Transfer in Chemistry, Vol. I: Principle and Theories*; Balzani, V., Ed.; Wiley-VCH: New York, 2001 (c) Mattay, J. In *Electron Transfer in Chemistry, Vol. II. Organic Molecules*; Balzani, V., Ed.; Wiley-VCH: New York, 2001. (d) Fukuzumi, S. *Org. Biomol. Chem.* **2003**, *1*, 609.
(18) Strictly speaking, the substitution-*stable* Creutz/Taube mixed-valence complex[8a] is a suitable electronic but a limited (kinetics) model for a precursor complex in *intermolecular* (diffusive) electron-transfer processes.
(19) Mulliken, R. S. *J. Phys. Chem.* **1952**, *56*, 801.
(20) Mulliken, R. S.; Person, W. B. *Molecular Complexes*. Wiley: N.Y. 1969.
(21) (a) Foster, R. *Organic Charge-Transfer Complexes*; Academic Press: New York, 1969. (b) Andrews, L. J.; Keefer, R. M. *Molecular Complexes in Organic Chemistry*; Holden-Day: San Francisco, CA, 1964.
(22) Rosokha, S. V.; Kochi, J. K. *J. Am. Chem. Soc.* **2007**, *129*, 828.
(23) (a) Ganesan, V.; Rosokha, S. V; Kochi, J. K. *J. Am. Chem. Soc.* **2003**, *125*, 2559. (b) Sun, D.; Rosokha, S. V.; Kochi, J. K. *J. Am. Chem. Soc.* **2004**, *126*, 1388.
(24) (a) Historically, the electronic transitions associated with such [**D**, $\mathbf{D}^{+\bullet}$] complexes of aromatic π-donors and their cation radicals have been referred to as charge-resonance absorptions.[25−27] (b) The corresponding intervalence absorption of [$\mathbf{A}^{-\bullet}$, **A**] complexes have been recently observed and identified for olefinic and quinonoid π-acceptors and their associated anion radicals.[23a,28]
(25) (a) Badger, B.; Brocklehurst, B. *Nature* **1968**, *219*, 263. (b) Badger, B.; Brocklehurst, B. *Trans. Faraday Soc.* **1969**, 65, 2582; **1970**, *66*, 2939.
(26) (a) Lewis, I. C.; Singer, I. C. *Chem. Phys.* **1965**, *43*, 2712. (b) Howarth, O. W.; Fraenkel, G. K. *J. Am. Chem. Soc.* **1966**, *88*, 4514.
(27) (a) Fritz, H. P.; Gebauer, H.; Friedrich, P.; Ecker, P.; Artes, R.; Schubert, V. *Z. Naturforsch.* **1978**, *336*, 498. (b) Chi, X.; Itkis, M. E.; Reed, R. W.; Oakley, R. T.; Cordes, A. W.; Haddon, R. C. *J. Phys. Chem. B* **2002**, *106*, 8278.
(28) (a) Rosokha, S. V.; Lu, J.-M.; Newton, M. D.; Kochi, J. K. *J. Am. Chem. Soc.* **2005**, *127*, 7411. (b) Rosokha, S. V. Newton, M. D.; Head-Gordon, M.; Kochi, J. K. *Chem. Phys.* **2006**, *326*, 117.
(29) Sun, D.-L.; Rosokha, S. V.; Kochi, J. K. *J. Phys. Chem B* **2007**. In press (Sutin issue).

Table 1. Redox Potentials of Donors and Acceptors and the Spectral Characteristics of Their Cation and Anion Radicals

N	Structure	Acronym	E^o, (V vs SCE) [a]	λ_{max}, nm (log ε)[a, b]
		Donors and their cation radicals.		
1a	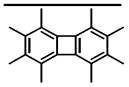	**OMB**	0.82[c]	596 (4.1)
2	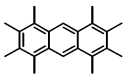	**OMA**	0.88	476 (4.0) 909 (3.9)
3a	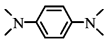	**TMPD**	0.12	567, 617 (4.1)
3b	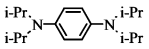	**TPPD**	0.09	577, 620 (4.1)
4a	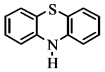	**PTZ**	0.59	520 (3.8), 747, 834
4b	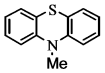	**MePTZ**	0.71	516(4.0), 780, 870
4c	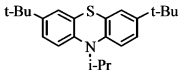	**PrPTZ**	0.70	570(4.0), 780, 860
5a		**DMB**	1.17	435, 460 (3.8)
5b	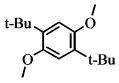	**DBB**	1.16	440, 467(3.9)
6		**TTF**	0.37	440 (4.2), 579
		Acceptors and their anion-radicals.		
7		**TCNE**	0.17	428 (3.9)[vs]
8		**DDQ**	0.52	460, 547, 587(3.8)
9	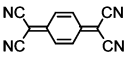	**TCNQ**	0.10	750, 850 (4.6)

[a] In CH_2Cl_2, at 295 K. [b] In parentheses $-\log \epsilon$ for the most intense band. [c] Oxidation wave split at low temperature.

prepared as the *closo*-dodecamethylcarboranate (CB^-) salts depicted in Chart 2, in which the negative charge is known to be extensively delocalized over the large quasi-spherical anion to allow only *separated ion pairs* (SIP) to be formed in solution and in the crystalline solid state.[30] Likewise, all anion radicals for eq 1b were prepared as SIP salts of the ligated potassium counterion $K(L)^+$, wherein the three-dimensional $L = [2,2,2]$ cryptand completely encapsulates the alkali-metal cation sufficient to isolate it from the anion radicals in Table 1.[31,32]

2.1. Preparation and Characterization of Ion-Radical Salts of Electron Donors and Acceptors. The electronic coupling

(30) (a) Sun, D.-L.; Rosokha, S. V.; Kochi, J. K. *Angew. Chem.* **2005**, *44*, 5133. (b) Rosokha, S. V.; Neretin, I. S.; Sun, D.-L.; Kochi, J. K. *J. Am. Chem. Soc.* **2006**, *128*, 9394.

(31) Lu, J. M.; Rosokha, S. V.; Lindeman, S. V.; Neretin, I. S.; Kochi, J. K. *J. Am. Chem. Soc.* **2005**, *127*, 1797.

(32) Lu, J. M.; Rosokha, S. V.; Neretin, I. S.; Kochi, J. K. *J. Am. Chem. Soc.* **2006**, *128*, 16708.

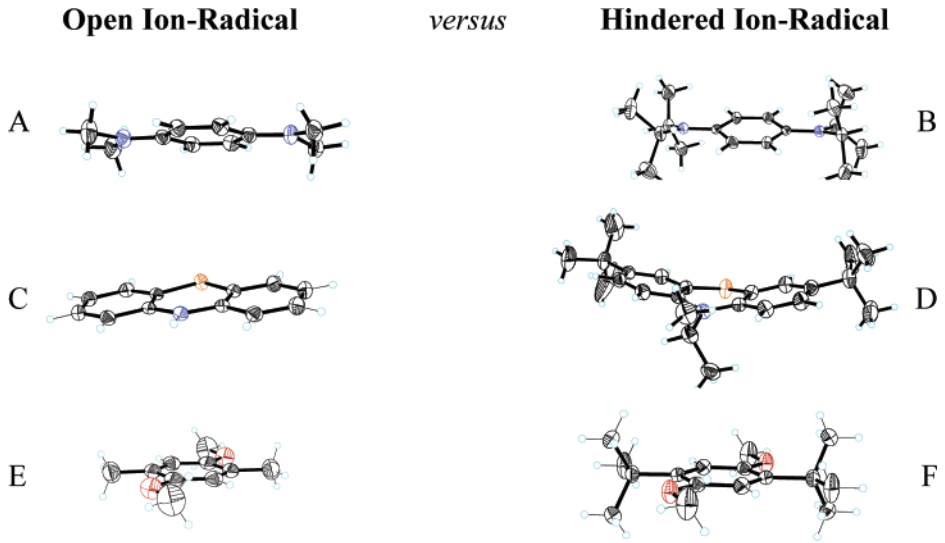

Figure 1. Molecular structures of sterically open and hindered (closed) cation radicals: (A) **TMPD**$^{+\bullet}$ vs (B) **TPPD**$^{+\bullet}$; (C) **PTZ**$^{+\bullet}$ vs (D) **PrPTZ**$^{+\bullet}$; (E) **DMB**$^{+\bullet}$ vs (F) **DBB**$^{+\bullet}$ [note that (B) to (F) are taken from X-ray structures of the corresponding **D**$^{+\bullet}$CB^{-} salts and (A) taken from **TMPD**$^{+\bullet}$**TCNE**$^{-\bullet}$[29]].

Chart 2

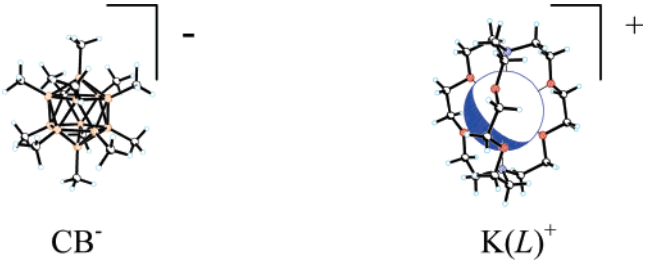

effects on the electron-transfer self-exchange of various cation and anion radicals were based on the donor and acceptor systems illustrated in Table 1. This donor and acceptor array included aromatic as well as olefinic systems that are open for intermolecular interactions as well as those containing the same (redox) core but sterically hindered with bulky substituents.[33] All electron donors and acceptors were characterized in dichloromethane solution by reversible cyclic voltammograms, the $E°$ values of which are included in the third column. Of particular interest is the aromatic donor **OMB** which exhibited an unusual splitting of the anodic wave at low temperatures (see Figure S1 in Supporting Information); the mechanistic implication of this unusual behavior will be discussed below.

Crystalline cation-radical salts of the electron donors were prepared by direct one-electron oxidation with stoichiometric amounts of the *closo*-dodecamethylcarboranyl radical (CB$^{\bullet}$),[34] nitrosonium salt ($NO^{+}SbCl_6^{-}$),[35] or simply pentachloroantimony[36] to produce large (encumbered) counter anions. The availability of such crystalline salts allowed the following: (i) high kinetic stability (persistency) of the cation radical sufficient for accurate measurements, (ii) good solubility in the noncoordinating (moderately polar) dichloromethane to lessen solvent effects, and (iii) minimum counterion interaction for the cation radicals to exist as separate ions with minimal ion-pairing effects. Likewise, crystalline anion-radical salts of the electron acceptor in Table 1 were prepared as the potassium cation totally encased within the cavity of a three-dimensional polyether ligand by potassium-mirror reduction in the presence of [2,2,2]cryptand in THF solutions. In all cases, the pure salts were easily separated in nearly quantitative yield by the addition of hexane, and their purities established by spectral titration were found to be >98%.

The remote introduction of bulky *tert*-butyl (^{t}Bu) or isopropyl (^{i}Pr) substituents into the organic donors caused only a relatively minor perturbation of either the redox potential or the spectral (UV−vis) characteristics of the redox core, as illustrated by the comparison of the entries for phenylenediamine (**3b** vs **3a**), phenothiazine (**4c** vs **4b**), and quinol ether (**5b** vs **5a**) in Table 1. In each case, the basic structural changes established by X-ray crystallographic analysis of crystalline salts (see Experimental Section) from the one-electron oxidation of the sterically hindered donor (Figure 1) are quite similar to those found in the parent (planar) donors. For example, the oxidation of tetramethyl-*p*-phenylendiamine (**TMPD**) to its cation radical leads to (i) shortening of the C_{ar}−N bond from 1.41 to 1.36 Å, (ii) significant quinonoid distortion of the aromatic ring so that the essentially equivalent (C−C) bonds of 1.40 Å become significantly different (1.42 and 1.36 Å), and (iii) planarization of the amino group becomes essentially complete, so that the sum of the internal C−N−C angles are 359.6° in the cation radical. Similarly, the oxidation of the tetra-isopropyl-substituted analogue (**TPPD**) leads to similar changes, i.e., (i) the shortening of the C_{ar}−N bond from 1.42 to 1.36 Å; (ii) quinonoid distortion of the aromatic ring so that the nearly equivalent aromatic bonds (∼1.40 Å) in the neutral donor become nonequivalent (1.42 and 1.36 Å);[37] and (iii) the planarization of the amino group, so

(33) For steric effects on the diffusive (charge-transfer) association of organic and organometallic electron donor/acceptor dyads, see: (a) Wong, C. L.; Kochi, J. K. *J. Am. Chem. Soc.* **1979**, *101*, 5593. (b) Fukuzumi, S.; Wong, C. L.; Kochi, J. K. *J. Am. Chem. Soc.* **1980**, *102*, 2928. (c) Hubig, S. M.; Rathore, R.; Kochi, J. K. *J. Am. Chem. Soc.* **1999**, *121*, 610. (d) Rathore, R.; Lindeman, S. V.; Kochi, J. K. *J. Am. Chem. Soc.* **1997**, *119*, 9393.

(34) King, B. T.; Noll, B. C.; McKinley, A. J.; Michl, J. *J. Am. Chem. Soc.* **1996**, *118*, 10902.

(35) (a) Rathore, R.; Kochi, J. K. *Acta Chem. Scand.* **1998**, *52*, 114. (b) Rosokha, S. V.; Kochi, J. K. *J. Am. Chem. Soc.* **2001**, *123*, 8985.

(36) Rathore, R.; Kumar, A. S.; Lindeman, S. V.; Kochi, J. K. *J. Org. Chem.* **1998**, *63*, 5847.

(37) (a) For quantitative (structural) evaluations of the quinonoidal distortion of benzenoid rings upon one-electron oxidation and reduction, see the Pauling-based bond-length/bond-order analysis: (b) Lindeman, S. V.; Rosokha, S. V.; Sun, D.; Kochi, J. K. *J. Am. Chem. Soc.* **2002**, *124*, 843 and Lu J. M., et al. in ref 32.

that the sum of the C−N−C angles increases from 341.2° in the neutral donor to 359.8° in the cation radical.

Structural changes upon oxidation of the sterically hindered phenothiazine and dimethoxybenzene donors, **PrPTZ** and **DBB**, are also comparable to those in the unhindered parents: **PTZ** and **DMB**, respectively. Thus, the oxidation of phenothiazine results in (i) the shortening of the S−C bond from 1.76 to 1.71 Å in **PTZ** and from 1.77 to 1.73 Å in **PrPTZ**; (ii) shortening of N−C bonds from 1.40 Å to 1.38 Å in **PTZ** and from 1.42 Å to 1.40 Å in **PrPTZ**; and (iii) planarization, so the angle between aromatic planes increases from 158° to 176° in **PTZ** and from 140° to 158° in **PrPTZ**. In the dimethoxybenzenes, one-electron oxidation leads to (i) the shortening of the C_{ar}−O bonds (1.38 Å) in the neutral donor to 1.32 Å in the cation radical, (ii) the quinonoidal distortion of the benzene ring consisting of essentially equivalent bonds (∼1.39 Å) in the neutral donor to inequivalent bonds of 1.44/1.36 Å in the cation radicals, and (iii) the coplanarization of the methoxy group with respect to the aromatic plane.[38]

Spectral, electrochemical, and structural data thus indicate that the thermodynamics of the redox processes, as well as the geometric changes upon oxidation, and spectral properties of ion radicals of hindered systems are close to those of planar species that are sterically "open" for π-interactions. Let us now compare how such π-interactions affect the dynamics of electron-transfer self-exchange.

2.2. EPR Studies of Ion Radicals and the Electron-Transfer (ET) Kinetics of the Self-Exchange Processes. Dissolution of the pure ion-radical salts (Table 1) in dichloromethane at room temperature formed the basis of our quantitative rate measurements since earlier studies principally by Weissman and co-workers[39] defined the self-exchange kinetics via their diagnostic EPR linebroadening behavior. Indeed, our measurements based on the isolation of pure ion-radical salts (see Experimental Section) consistently afforded well-resolved EPR spectra, the hyperfine splitting constants of which were basically within the experimental errors.[40,41] Most importantly, the incremental addition of either the neutral donor (**D**) to the cation radical ($\mathbf{D}^{+\bullet}$) or the neutral acceptor (**A**) to the anion radical ($\mathbf{A}^{-\bullet}$) generally led to the same characteristic progressive linebroadening (slow-exchange limit) observed earlier.[42] As a result, the further addition of the diamagnetic parent induced the collapse of the resolved EPR spectrum of the ion radical into a single broad envelope which then characteristically narrowed in the final fast-exchange limit (see Figure S2 for representative examples). Such well-known linebroadening effects resulted from the intermolecular electron-transfer self-exchange as described by eqs 1a and 1b (vide supra). Thus following the earlier studies,[43] we determined the second-order rate constants (see Experimental Section for details) based on the line width variation with changing concentrations of the diamagnetic parent, and the self-exchange values of k_{SE} are included in Table 2 for the parent cation radicals and anion radicals as well as their sterically hindered derivatives.[44]

The results in Table 2 revealed four salient structural facets of the ion-radical kinetics for the self-exchange process. First, limiting second-order rates that were uniformly close to the fast-exchange limit of $k_{SE} \approx (3-5) \times 10^9$ M^{-1} s^{-1} in Table 2 were attained by all the unsubsituted ("open") cation and anion radicals. Second, the activation energies for ET self-exchange of the open ion radicals as evaluated from the linear dependence of ln k_{SE} with inverse temperature lay in the range $E_a \approx 1-3$ kcal mol^{-1} that is generally in accord with the diffusion barrier of $E_{diff} \approx 2.5$ kcal mol^{-1}.[45] Third, of the various donor/acceptor systems described in Table 1, the octamethylbiphenylene (**OMB**/$\mathbf{OMB}^{+\bullet}$) dyad was unique in that the temperature dependence of the second-order rate constant ln k_{SE} with T^{-1} was distinctly nonlinear. Most revealingly, when solutions of $\mathbf{OMB}^{+\bullet}$ with added **OMB** were progressively cooled, the EPR spectra showed the appearance of additional hyperfine lines so that, at the lowest temperature of −90 °C, the EPR spectrum simply consisted of doubled lines with halved hyperfine splittings that were diagnostic of the completely delocalized dimeric species: $(\mathbf{OMB})_2^{+\bullet}$ structurally (X-ray) identified earlier.[41a] Fourth, their sterically hindered ("closed") analogues with *tert*-butyl or isopropyl substituents were consistently slower by several orders of magnitude in comparison with their more "open" parents. As such, the clear distinction between the self-exchange kinetics of the open versus the sterically hindered ion radicals caused us to closely examine the intermolecular interaction with their diamagnetic parents in greater detail, as follows.

2.3. Spontaneous Association of Ion Radicals with their Diamagnetic Parents. Formation of Transient 1:1 Complexes. The facile association of ion radicals with their diamagnetic parents was experimentally observed spectroscopically as intermolecular 1:1 associates, hereinafter referred to as transient complexes (TCs).[22,23] For example, dichloromethane solutions of all the ion radicals in Table 1 were characterized by intense absorptions in the UV−vis spectral region, but the colored solutions were completely transparent in the near-IR region between 1000 and 3000 nm. On the other hand, when the diamagnetic parent was added, a new absorption band could be detected immediately in the NIR region (Figure 2), typically at $\lambda_{max} = 1900$ nm with the extinction coefficient $\epsilon_{max} = 1700$

(38) Rathore, R.; Kochi, J. K. *J. Org. Chem.* **1995**, *60*, 4399.
(39) (*a*) Ward, R. L.; Weissman, S. I. *J. Am. Chem. Soc.* **1957**, *79*, 2086. (b) Phillips, W. D.; Rowell, J. C.; Weissman, S. I. *J. Chem. Phys.* **1960**, *33*, 626.
(40) For example, the values of the EPR hyperfine splittings of the cation radicals are (in G): 4.5 (12H) for $\mathbf{OMB}^{+\bullet}$;[41a] 5.45 (2H), 3.34 (12H), and 1.67 (12H) for $\mathbf{OMA}^{+\bullet}$;[41a] 7.05 (2N), 2.0 (4H), and 6.8(12H) for $\mathbf{TMPD}^{+\bullet}$;[41b] 7.15 (2N) and 1.9 (4H) for $\mathbf{TPPD}^{+\bullet}$;[41b] 4.37 (6H), 3.12(6H), and 0.48 (2H) for $\mathbf{DMD}^{+\bullet}$;[41c] 1.23 (4H) for $\mathbf{TTF}^{+\bullet}$;[41d] etc.
(41) (a) Kochi, J. K.; Rathore, R.; Le Magueres, P. *J. Org. Chem.* **2000**, *65*, 6826. (b) Grampp, G.; Kelterer, A.-M.; Landgraf, S.; Sacher, M.; Niethammer, D.; Telo, J. P.; Dias, R. M. B.; Vieira, A. J. S. C. *Monatsh. Chem.* **2005**, *136*, 519. (c) Forbes, W. F.; Sullivan, P. D. *J. Phys. Chem.* **1968**, *48*, 1411. (d) Khodorkovsky, V.; Shapiro, L.; Krief, P.; Shames, A.; Mabon, G.; Gorgues A.; Giffard, M. *Chem. Commun.* **2001**, 2736.
(42) Note that the rate constants for electron-transfer self-exchange for most of the ion radicals from Table 1 are available in the literature.[23b,43] However, the reported values were generally obtained with ion radicals prepared in situ in various solvents and with different counterions. Accordingly, to exclude solvent and counterion effects, we have remeasured all the rate constants using consistently pure ion-radical salts with bulky counterions in the same noncoordinating solvent, i.e., the moderately polar dichloromethane.
(43) (a) Kowert, B. A.; Marcoux, B. A.; Bard, A. J. *J. Am. Chem. Soc.* **1972**, *94*, 5538. (b) Grampp, G. *Spectrochim. Acta* **1998**, *A54*, 2349. (c) Grampp, G.; Jaenicke, W. *Ber. Bunsen. Phys. Chem.* **1991**, *95*, 904. (d) Jurgen, D.; Pedersen, S.; Pedersen, J. A.; Lund, H. *Acta Chem. Scand.* **1997**, *51*, 767. (e) Eberson, L. *Adv. Phys. Org. Chem.* **1982**, *18*, 79. (f) Grampp, G.; Harrer, W.; Hetz, G. *Ber. Buns. Phys. Chem.* **1990**, *94*, 1343.
(44) The self-exchange kinetics of the sterically hindered ion radicals were more difficult to measure, and thus the values of k_{SE} were somewhat less accurate owing to the more complex hfs patterns with overlapping lines (slow exchange limit). Moreover, the relatively slow second-order rate constants of these closed ion radicals prevented their approach to the fast exchange limit (see details in the Experimental Section).
(45) Calvert, J. G.; Pitts, J. N. *Photochemistry;* Wiley: New York, 1966; p 627.

Table 2. Rates Constants and Effective Activation Energies of the Electron-Transfer Self-Exchange Reaction of Ion Radicals[a]

N		Ion-radicals	k_{SE}, ($M^{-1}s^{-1}$)	$-E_a$, (kcal/mol)
1a	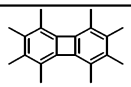	**OMB$^{+\bullet}$**	2.4×10^{9}	~ 4[g]
2	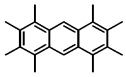	**OMA$^{+\bullet}$**	2.5×10^{9}[b]	0.4[b]
3a	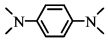	**TMPD$^{+\bullet}$**	2.3×10^{9}	~ 4[b]
3b	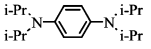	**TPPD$^{+\bullet}$**	1×10^{7}	-
4a	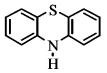	**PTZ$^{+\bullet}$**	4.7×10^{9}	2.2[b]
4b	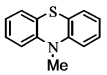	**MePTZ$^{+\bullet}$**	1.3×10^{9}[c]	-
4c	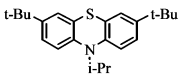	**PrPTZ$^{+\bullet}$**	3×10^{8}	-
5a		**DMB$^{+\bullet}$**	1.5×10^{9}	1.7[b]
5b	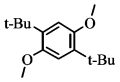	**DBB$^{+\bullet}$**	1×10^{8}	-
6		**TTF$^{+\bullet}$**	2.7×10^{9}[d]	0.9[d]
7		**TCNE$^{-\bullet}$**	4.3×10^{9}[e]	2.0[e]
8		**DDQ$^{-\bullet}$**	2.5×10^{9}	1.6[f]
9	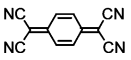	**TCNQ$^{-\bullet}$**	3.3×10^{9}	1.9[f]

[a] Measured in CH_2Cl_2 at 295 K, with CB^- or K(*L*) $^+$ counterions, unless noted otherwise. [b] Measured with $SbCl_6^-$ counterion. [c] From ref 46. [d] From ref 22. [e] From ref 28b. [f] NBu_4^+ counterion. [g] Doubled EPR spectrum at low temperature.[41a]

M^{-1} cm^{-1} for the phenothiazine cation radical.[46,47] The intensity of the new NIR absorption increased upon further additions of the diamagnetic parent, and it also showed significant enhancement as the temperature was lowered (Figure S4 in the Supporting Information). Considerable differences in the NIR-absorption intensity were apparent with various ion-radical pairs. For example, the octamethylbiphenylene system (**OMB/OMB$^{+\bullet}$**) showed intense NIR bands at $\lambda_{max} = 1850$ nm,[41a] whereas the tetramethyl-*p*-phenylenediamine pair (**TMPD/TMPD$^{+\bullet}$**) afforded only a weak but quite distinct absorption in NIR region ($\lambda_{max} = 1050$ nm) at the same concentrations (Figure S3 in the Supporting Information). Comparable spectral data are tabulated in Table 3 (columns 3 and 4) for the transient complexes of all the open cation− and anion radicals. However, detailed comparisons confirmed that the sterically hindered (closed) pairs showed no evidence for complex formation since their parent/ion-radical mixtures were completely transparent in the NIR region between 1000 and 3000 nm, even at the highest attainable concentrations and at very low temperatures.

Quantitative analysis of the absorption intensity with changing concentrations of the parent/ion-radical combinations followed

(46) See Sun D.-L., et al. in ref 23b.
(47) Note that similar NIR absorption bands were observed in other solvents, such as acetonitrile, acetone, THF, etc. The solvent dependence of such systems will be reported later in detail.

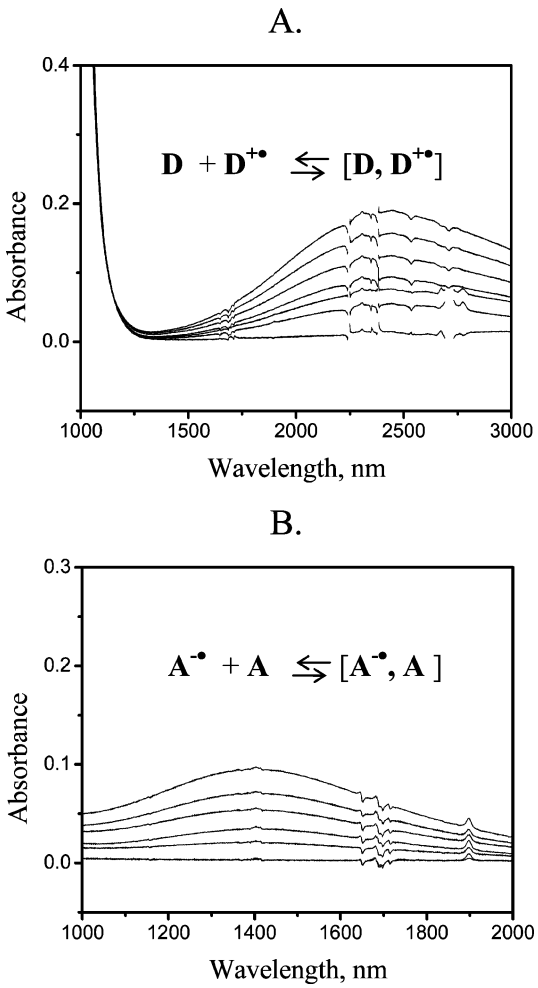

Figure 2. Typical spectral changes in NIR range attendant upon addition of neutral parents to their ion radicals in dichloromethane (l = 1 mm, 22 °C). (A) 2.1 mM **OMA**$^{+\bullet}$CB and (from bottom to top) 0, 0.7, 1.0, 1.5, 2.0, 3.0, 4.0 mM **OMA**. (B) 5.5 mM of K(L)$^{+}$**DDQ**$^{-\bullet}$ and 0, 1.6, 3.0, 4.6, 6.0, 8.0 mM of **DDQ**.

the pattern established earlier for the formation of cationic as well as the anionic complexes according to eqs 3 and 4, respectively,

$$\mathbf{D} + \mathbf{D}^{+\bullet} \overset{K_\pi}{\rightleftharpoons} [\mathbf{D}, \mathbf{D}^{+\bullet}] \quad (3)$$

$$\mathbf{A}^{-\bullet} + \mathbf{A} \overset{K_\pi}{\rightleftharpoons} [\mathbf{A}^{-\bullet}, \mathbf{A}] \quad (4)$$

for which typical intensity changes of the NIR absorption bands are illustrated in Figure 2. The equilibrium constant (K_π) for complex formation derived from the concentration dependence studies are included in column 5 of Table 3 (see Experimental Section for details). The linear dependence of ln K_π with inverse temperature (see inset Figure S3) afforded the thermodynamic parameters ΔH_π and ΔS_π which are listed in columns 6 and 7 (Table 3).

2.4. Isolation and X-ray Structure of the Ion-Radical Transient Complex. Dissolution of the crystalline potassium salt of the dichlorodicyanoquinone anion radical (K^{+}**DDQ**$^{-\bullet}$)[43] in dichloromethane was accomplished by the addition of the polyether ligand (benzo-15-crown-5) and was followed by the addition of equimolar amounts of the parent acceptor (**DDQ**). This dark green solution was simply cooled to −65 °C and

Table 3. Thermodynamics of Ion-Radical Associations with Their Parent (eqs 3 and 4) and Spectral Characteristics (NIR Intervalence Band) of the Dimeric Species: $\mathbf{D}_2^{+\bullet}$ or $\mathbf{A}_2^{-\bullet}$[a]

	transient complex	λ_{max} (nm)	ϵ_{max} (M^{-1} cm^{-1})	K_π (M^{-1})	$-\Delta H_\pi$ (kcal/mol)	$-\Delta S_\pi$ (eu)
1a	$(\mathbf{OMB})_2^{+\bullet}$	1850	5700	350	2.5[b]	2[b]
2	$(\mathbf{OMA})_2^{+\bullet}$	2430	5000	60	5.7[b]	12[b]
3a	$(\mathbf{TMPD})_2^{+\bullet}$	1050	1150	0.1	1.3[b]	4[b]
3b	$(\mathbf{TPPD})_2^{+\bullet}$	*c*				
4a	$(\mathbf{PTZ})_2^{+\bullet}$	1900	1700	3	2.4[b]	4[b]
4b	$(\mathbf{MePTZ})_2^{+\bullet}$	*c*				
4c	$(\mathbf{PrPTZ})_2^{+\bullet}$	*c*				
5a	$(\mathbf{DMB})_2^{+\bullet}$	1850	530	0.9[b]	3.2[b]	10[b]
5b	$(\mathbf{DBB})_2^{+\bullet}$	*c*				
6	$(\mathbf{TTF})_2^{+\bullet}$	2115	5000	6	5.5	16
7	$(\mathbf{TCNE})_2^{-\bullet}$	1515	1000	4.5	3.4	8.5
8	$(\mathbf{DDQ})_2^{-\bullet}$	1406	3000	11	3.2	6
9	$(\mathbf{TCNQ})_2^{-\bullet}$	2200	3200	5	3.3	7

[a] Measured in CH_2Cl_2 at 295 K, with $CB^{-\bullet}$ or K(L)$^{+}$ counterions, unless noted otherwise. [b] With $SbCl_6^-$ [c] TC not observed (see text).

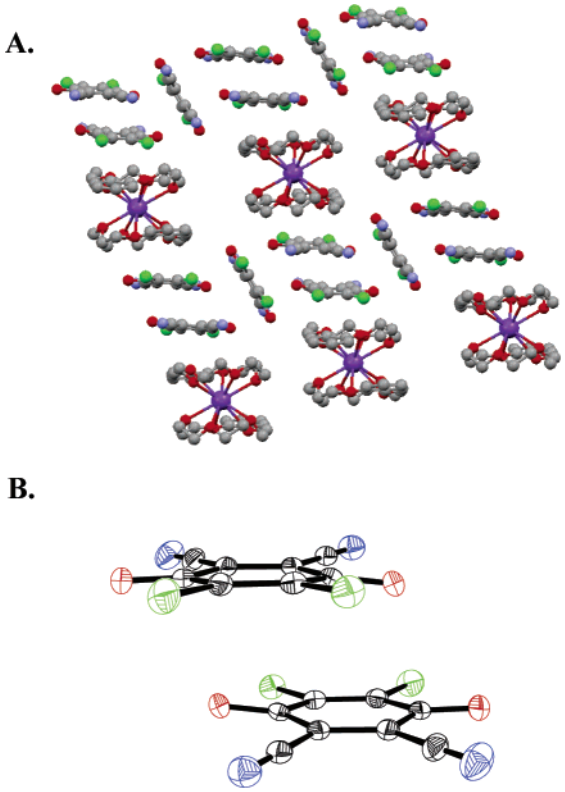

Figure 3. (A) Crystal lattice of the dimeric units formed by two partially charged **DDQ** moieties with hydrogens and solvent molecules omitted for clarity. (B) Details of the transient complex (TC) of **DDQ** and **DDQ**$^{-\bullet}$.

carefully overlaid with hexane, and the mixture was allowed to stand undisturbed for several weeks, whereupon it deposited dark brown crystals, the X-ray crystallographic analysis of which revealed the triclinic unit cell to contain three independent **DDQ** forms, hereinafter referred to as *A*, *B*, and *C* and paired with the completely encapsulated potassium counterion K(15-crown-5)$_2^{+}$ shown in Figure 3A. Forms *A* and *B* constitute a pair of quite similar centrosymmetric dimeric units shown in Figure 3B, in which the **DDQ** moieties lie parallel to each other at the close interplanar separation of r_π = 2.95 Å (in form *A*) and 2.97 Å (in form *B*). In the crystal lattice, these dimeric units are interchangeable with the bis-ligated potassium counterion, as illustrated in Figure 3A. The third (more isolated) form *C* consists of the monomeric **DDQ** unit that is separately arranged

between the stacks formed by interchanging dimeric units and $[K(15crown5)_2]^+$.

To determine the distribution of the overall negative (−1) charge between the **DDQ** moieties, they were analyzed in comparison with those of the parent **DDQ** and its separated anion radical **DDQ**$^{-\bullet}$. Such an analysis indicated that the geometry of the separate species *C* is essentially that of the neutral acceptor (see Table S2 in the Supporting Information). On the other hand, both *A* and *B* forms show elongated C═O and C═C double bonds and with the C−C single bond shortened relative to that in the neutral acceptor. [The latter corresponds to an increase of the electron density in the LUMO.] Moreover, quantitative analysis similar to that in other benzoquinone systems examined earlier[48] (see Supporting Information for details) indicated that each **DDQ** moiety in species *A* and *B* bears one-half a negative charge to verify the overall (−1) charge on each of the dimeric units. Most important for the present study is the fact that geometries of these dimeric **DDQ** units show the following: (i) the interplanar π-separations of 2.97 and 2.95 Å which are quite similar to those observed in several diamagnetic dianionic dimers of **DDQ** and its dianionic triplex associates;[23a] and (ii) the lateral shifts of ∼1.8 Å parallel and ∼0.4 Å perpendicular to the O−O axis, as also observed in other associates.[49]

The unit cell shown in Figure 3A clearly demonstrates the existence of discrete dimeric units of the **DDQ** moiety in the crystalline complex. As such, its cofacial or face-to-face (slightly slipped) π-stacking at the interplanar separation of $r_\pi \approx 3$ Å is strongly related to those of analogous ion-radical assemblies observed with octamethylbiphenylene,[50] tetracyanoquinodimethane,[51] and tetrathiafulvalene,[22] in which the dimeric units (**OMB**)$_2^{+\bullet}$, (**TCNQ**)$_2^{-\bullet}$, and (**TTF**)$_2^{+\bullet}$ have also been structurally characterized, but in less cleanly differentiated units. We also note that the crystallographic literature contains structural data of the other ion-radical salts listed in Table 1, but as other types of intermolecular associates that include dicationic and dianionic dimers as well as mixed-valence triads, pentads, and higher aggregates.[52] It is thus noteworthy that they are uniformly characterized by a common structural motif consisting of the parallel (cofacial) π-arrangements of planar entities (lying atop each other but somewhat shifted laterally) at interplanar separations that lie in a rather narrow range of $r_\pi \approx 3.0-3.3$ Å, which is notably 0.2−0.5 Å shorter than the sum of their van der Waals radii.[53] Furthermore, no pertinent structural distinction can be made between the paramagnetic (ion-radical) complexes established in this and other related systems from those of the diamagnetic (dimer) dications and dianions in the same family of ion radicals.[22,23]

Such a comprehensive analysis of the solid-state data leads us to conclude that the paramagnetic (mixed-valence) complexes such as (**DDQ**)$_2^{-\bullet}$ and (**TTF**)$_2^{+\bullet}$ share structural features in common with their diamagnetic (dimer) analogues, (**DDQ**)$_2^{2-}$[49] and (**TTF**)$_2^{2+}$,[22] and that the latter can be gainfully employed, especially when the former structure is experimentally unavailable (vide infra). The interplanar π-separation within the cofacial (1:1) array which is measurably less than their van der Waals radii, but subject to some lateral excursion, points to a rather shallow potential minimum or multiple, close-lying minima[22] to indicate that the same mutual arrangement of the ion radical with its neutral parent is also likely to coexist in solution. In such a case, we conclude that the cofacial arrangement and interplanar separation extant in the transient complex (TC) represent a reasonable approximation of the precursor complex (PC) in the electron-transfer self-exchanges of interest in this study.

2.5. Electronic Structures of the Transient Complexes. The well-defined electronic transitions in the NIR spectral region that characterize the ion-radical complexes in Table 3 allow the application of Mulliken−Hush (two-state) methodology[55] to establish values of the electronic coupling element (H_{DA}) and the reorganization energy (λ) for electron transfer within these 1:1 cation-radical and anion-radical associates, i.e.,

$$[\mathbf{D}, \mathbf{D}^{+\bullet}] \overset{ET}{\rightleftharpoons} [\mathbf{D}^{+\bullet}, \mathbf{D}] \text{ and } [\mathbf{A}^{-\bullet}, \mathbf{A}] \overset{ET}{\rightleftharpoons} [\mathbf{A}, \mathbf{A}^{-\bullet}] \quad (5)$$

However, such an analysis requires the prior assignment of both ion-radical complexes to either a localized (Class II) or delocalized (Class III) category within the Robin−Day classification.[56] Thus, in localized mixed-valence complexes, the reorganization energy is equal to the intervalence transition energy, i.e., $\nu_{IV} = \lambda_i + \lambda_s$ (where λ_i is the vibrational and the λ_s is solvent component of the reorganization energy), and it is solvent-dependent. The electronic coupling in such systems can be evaluated as[55]

$$H_{DA} = 0.0206(\nu_{IV}\, \Delta\nu_{1/2}\, \epsilon_{IV})^{1/2}/r_{DA} \quad (6)$$

where ν_{IV} and $\Delta\nu_{1/2}$ are the spectral maximum and full width at half-maximum (cm^{-1}) of the electronic (intervalence) band, ϵ_{IV} is its extinction coefficient (M^{-1} cm^{-1}), and r_{DA} is the separation (Å) between the (donor/acceptor) redox centers. On the other hand, in the delocalized complexes the electronic coupling is evaluated directly from the energy of the intervalence transition as $\nu_{IV} = 2H_{DA}$, and it is essentially *solvent-independent*.

We have already noted that, in some systems (e.g., **DMB**$^{+\bullet}$/**DMB**), the energies of the intervalence bands are notably higher in more polar solvents (such as DMF, acetonitrile, and acetone) than those measured in the less polar dichloromethane, whereas in some cases such as (**OMB**)$_2^{+\bullet}$ the NIR transitions are practically *solvent-independent*. We accordingly assigned the first group of ion-radical complexes to Robin-Day Class II, and the second to Class III in Table 4. Importantly, such an assignment is supported by ab initio computations of the electronic coupling and reorganization energies in various

(48) See Lu, J. M., et al. in ref 32.
(49) (a) Yan, Y.-K.; Mingos, M. P.; Muller, T. E.; Williams, T. E.; Kurmoo, M. *J. Chem. Soc., Dalton Trans* **1995**, 2509. (b) Marzotto, A.; Clemente, D. A.; Pasimeri, L. *J. Crystallogr. Spectrosc. Res.* **1988**, *18*, 545.
(50) Le Magueres, P.; Lindeman, S.; Kochi, J. K. *J. Chem. Soc., Perkin Trans. 2* **2001**, 1180.
(51) (a) Goldstein, P.; Seff, K.; Trueblood, K. N. *Acta Crystallogr*. **1968**, *B24*, 778. (b) Hanson, A. W. *Acta Crystallgr*. **1968**, *B24*, 773. (c) Kobayashi, H. *Bull. Chem. Soc. Jpn.* **1974**, *47*, 1346.
(52) Soos, Z. G.; Klein, D. J. In *Molecular Association*; Foster, R., Ed.; Academic Press: New York, 1975; Vol. 1.
(53) (a) The measurable contraction of the interplanar separation beyond their van der Waals radii[53b] is taken to represent the inner-sphere character of the intermolecular interaction as spectrally revealed by the charge-transfer transition. For a discussion of this important point, see Rathore, et al. in ref 33d. (b) Bondi, A. *J. Phys. Chem.* **1964**, *68*, 441.
(54) See Rosokha, S. V., et al. in ref 22.
(55) (a) Creutz, C.; Newton, M. D.; Sutin, N. *J. Photochem. Photobiol. A: Chem.* **1994**, *82*, 47. (b) Brunschwig, B. S.; Sutin, N. In *Electron Transfer in Chemistry*; Balzani, V., Ed.; Wiley: New York, 2001; Vol. 2, p 583.
(56) Robin, M. B.; Day, P. *Adv. Inorg. Chem. Radiochem.* **1967**, *10*, 247.

Table 4. Mulliken−Hush Analysis of the Electronic Interaction within the Transient π-Complex

	ion-radical π-complex	Class	r_π, Å	ν_{IV}, 10^3 cm^{-1}	$H_{DA,}$ 10^3 cm^{-1}
1	$(\mathbf{OMB})_2^{+\bullet}$	III	3.2	5.4	2.7[a]
2	$(\mathbf{OMA})_2^{+\bullet}$	III	3.3	4.1	2.1[a]
3a	$(\mathbf{TMPD})_2^{+\bullet}$	II	3.1	9.5	1.7[b]
4a	$(\mathbf{PTZ})_2^{+\bullet}$	II	3.2	5.3	1.1[b]
5a	$(\mathbf{DMB})_2^{+\bullet}$	II	3.2	5.4	0.7[b]
6	$(\mathbf{TTF})_2^{+\bullet}$	II	3.4	4.7	1.6[b]
7	$(\mathbf{TCNE})_2^{-\bullet}$	II	3.0	7.2	1.1[b]
8	$(\mathbf{DDQ})_2^{-\bullet}$	II/III	2.9	7.1	3.6[a] (1.8)[b]
9	$(\mathbf{TCNQ})_2^{-\bullet}$	II/III	3.2	4.6	2.3[a] (1.4)[b]

[a] $H_{DA} = \nu_{IV}/2$. [b] From eq 6.

Table 5. Computed[a] Reorganization Energies and Coupling Elements for the Mixed-Valence Ion-Radical Complexes in Comparison with Experimental[b] (Spectral) Values

	transient complex	λ^{calcd} (10^3 cm^{-1})	λ^{expt} (10^3 cm^{-1})	$H_{DA}{}^{a}$ (10^3 cm^{-1})	$H_{DA}{}^{expt\ b}$ (10^3 cm^{-1})
1	$(\mathbf{OMB})_2^{+\bullet}$	4.0 (6.2)	-	2.3 (3.2)	2.7
2	$(\mathbf{OMA})_2^{+\bullet}$	2.5 (4.9)	-	- (3.3)	2.1
3a	$(\mathbf{TMPD})_2^{+\bullet}$	5.7 (10.5)	9.5	2.6 (3.7)	1.7
5a	$(\mathbf{DMB})_2^{+\bullet}$	5.8	5.4	2.5	0.7
6	$(\mathbf{TTF})_2^{+\bullet}$[c]	4.4	4.7	3.6	1.6
7	$(\mathbf{TCNE})_2^{-\bullet}$[d]	4.4 (6.6)	6.6	4.2 (7.2)	1.1
8	$(\mathbf{DDQ})_2^{-\bullet}$	5.5 (9.4)	7.1	3.4 (4.8)	3.6 (1.8)

[a] B3LYP calculation and the Hartree−Fock calculation in parentheses. [b] See Table 4. [c] From ref 22. [d] From ref 28b.

complexes (vide infra). Additionally, this assignment is consistent with the larger formation constants of Class III complexes, and this is confirmed by the observation of the "doubled" ESR spectrum of the $(\mathbf{OMB})_2^{+\bullet}$ π-complex (vide supra).[41a]

For Class II complexes, we thus calculated the electronic coupling element H_{DA} from eq 6 based on the spectral characteristics of the NIR band using the separation parameter (r_π) taken from solid-state data, and the reorganization energy was equated to the energy of NIR transition. For Class III complexes, the coupling energy was determined directly from the intervalence transition as $H_{DA} = \nu_{IV}/2$. The data are presented in the last column of Table 4.

Since the corresponding spectral data for the ion-radical complexes of the sterically hindered analogues were experimentally unavailable owing to the very limited magnitude of their formation constant (K_π in Table 3) sufficient to allow their isolation, we next turned to several quantum-mechanical methods to compute estimates of the electron-transfer parameters λ and H_{DA}. Before proceeding further, however, it was necessary to evaluate the reliability of the theoretical methods by first comparing the computed values of λ and H_{DA} with the corresponding experiment-based values obtained from the spectral data and eq 6 as follows.

2.6. Computations of the Reorganization (λ) and Electronic Coupling (H_{DA}) Energies. 2.6.1. Reorganization Energy. The intramolecular component (λ_i) was calculated as the energy difference between the initial diabatic state with the electron located on the donor (with reactants in their relaxed geometries) and the final diabatic state (with the same nuclear geometry but the electron transferred to the acceptor)[57] see Experimental Section for details. The solvent reorganization energy (λ_o) for electron transfer within the ion-radical complex was based on the solvent cavity of radii a_o with an internal dielectric constant of $\epsilon_{in} = 2$ immersed in medium with static and optical dielectric constants ϵ_s and ϵ_o, respectively, using the Kirkwood solvation model.[28,58] The estimated values of the reorganization energies are listed in Table 5 for several ion-radical complexes in dichloromethane (for computational details of λ_i and λ_o, see the Experimental Section and Supporting Information).

2.6.2. Electronic Coupling Element. Theoretical evaluations of H_{DA} for the ion-radical complexes were based on the energy splitting resulting from the symmetric and antisymmetric combinations of the localized molecular orbitals of the monomers, as described earlier.[59] Thus in the cation-radical complex, the electronic coupling element was calculated as one-half of the energy difference between the HOMO and HOMO-1 (resulting from the pairwise splitting of the HOMO orbital of the parent donor) in the neutral closed-shell dimer. Likewise, in the anion-radical complex, H_{DA} was calculated as one-half of the energy difference between the LUMO + 1 and LUMO (resulting from orbital splitting of the acceptor LUMO in the corresponding neutral dimer).[60] The computed values (see Experimental Section and the Supporting Information for details) are listed in Table 5.

The comparative values of the computed reorganization energy (λ) and coupling element (H_{DA}) in Table 5 based on solid-state structures of the ion-radical complexes led us to several important conclusions. First, the results of the DFT calculations of the electronic coupling elements for Class III π-complexes agree well with those obtained from spectral data based on $H_{ab} = \nu_{IV}/2$ [note the experimental reorganization energies are unavailable for these types of ion-radical π-complexes]. Second, for Class II complexes, the experimental reorganization energies from the intervalence transition energy lie between the values obtained with the Hartree−Fock and the DFT-computed intramolecular reorganization component λ_i. However, the computed coupling elements are notably higher than those derived from the experimental (spectral) energies. The probable origin of such a discrepancy was discussed earlier, and it lies in either the uncertainty of the separation parameter r_π[61−63] or the labile nature of the ion-radical complex in solution,[64] or both. Such ambiguities notwithstanding, we conclude that the molecular-orbital computations are in reasonable agreement with the experimental (spectral) data, certainly sufficient to provide theoretical insight into the electronic coupling elements of the sterically hindered ion-radical complexes in the following way.

While bulky substituents generally prevent the close approach of sterically hindered moieties, the molecular modeling (MM) studies indicate that a pair of di-*tert*-butyl-substituted dimethoxybenzene (see **DBB** in Table 1) moieties can approach each other

(57) (a) Nelsen, S. F.; Blackstock, S. C.; Kim, Y. *J. Am. Chem. Soc.* **1987**, *109*, 677. (b) Perng, B.-C.; Newton, M. D.; Raineri, F. O.; Friedman, H. L. *J. Chem. Phys*. **1996**, *104*, 7153.
(58) Vener, M. V.; Ioffe, N. T.; Cheprakov, A. V.; Mairanovsky, V. G. *J. Electroanal. Chem.* **1994**, *370*, 33.
(59) Newton, M. D. *Chem. Rev.* **1991**, *91*, 767.
(60) Huang, J.-S.; Kertesz, M. *J. Chem. Phys.* **2005**, *122*, 234707.
(61) As noted recently,[62] the proper values of r_{DA} for the Mulliken−Hush equation may be significantly lower than that based on the geometric separation (r_π) of the redox centers, which implies that the correct coupling element may be up to 50% higher than that calculated from the crystallographic data.[63]
(62) (a) Newton, M. D. In *Electron Transfer in Chemistry*; Balzani, V., Ed.; Wiley-VCH, New York, 2001; Vol. 1, p 3 ff. (b) Nelsen, S. F.; Newton, M. D. *J. Phys. Chem. A* **2000**, *104*, 10023.
(63) See the discussion by Rosokha et al. in ref 22.

Chart 3

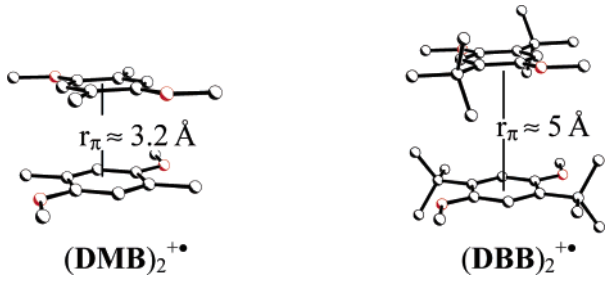

crosswise to an effective interplanar separation of ~5 Å without significant atomic overlap (Chart 3).

Roughly the same separation also pertains in the laterally shifted complex from tetraisopropyl-substituted *p*-phenylendiamine (TPPD). In order to estimate the values of the electronic coupling elements of the sterically hindered complexes, we computationally varied the interplanar separations (r_π) extant in those derived from the sterically open parents. In all cases, the increase in the interplanar separation resulted in an exponential decrease in the HOMO splitting as typically depicted in Figure 4.

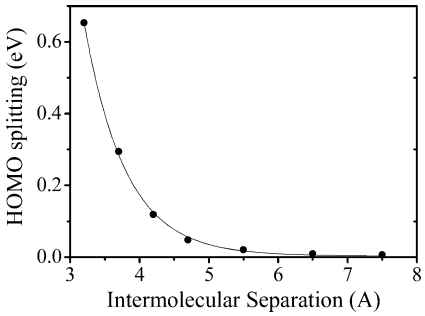

Figure 4. Exponential dependence of the HOMO splittings on the interplanar separation within $(\mathbf{TMPD})_2$ (calculated at the B3LYP/6-31G* level).

According to the calculations in Figure 4, the electronic-coupling characteristics of $H_{DA} \approx 100-300$ cm^{-1} are to be expected when the cofacial dyads are (artificially) arranged at an interplanar separation of $r_\pi \approx 5-5.5$ Å, and we have used these estimates (together with the reorganization energy taken from unhindered parents) in the kinetics analysis of the ET self-exchange processes for the ion radicals presented in Table 1.

3. Discussion

The spectral detection, isolation, and X-ray structures of the series of transient complexes in Figures 2 and 3 provide the critical links to the elucidation of the electron-transfer mechanism for the self-exchange processes in eqs 1 and 2, since they all pertain to identical experimental conditions of concentrations, temperatures, and solvents.

3.1. Generalized Formulation of the Electron-Transfer Kinetics for Ion-Radical Self-Exchanges. The direct melding of the second-order kinetics for eqs 1a and 1b with the equilibrium complex formation in eqs 3 and 4 leads to the composite mechanistic formulation in Scheme 1 which is equally applicable to cation radicals as well as to anion radicals as described in eqs 7 and 8, respectively.

Scheme 1

$$\mathbf{D} + \mathbf{D}^{+\bullet} \underset{}{\overset{k_{diff}}{\rightleftharpoons}} [\mathbf{D},\mathbf{D}^{+\bullet}] \overset{k_{ET}}{\rightleftharpoons} [\mathbf{D}^{+\bullet},\mathbf{D}] \overset{k_{sep}}{\rightleftharpoons} \mathbf{D}^{+\bullet} + \mathbf{D} \quad (7)$$

$$\mathbf{A}^{-\bullet} + \mathbf{A} \overset{k_{diff}}{\rightleftharpoons} [\mathbf{A}^{-\bullet},\mathbf{A}] \overset{k_{ET}}{\rightleftharpoons} [\mathbf{A},\mathbf{A}^{-\bullet}] \overset{k_{sep}}{\rightleftharpoons} \mathbf{A} + \mathbf{A}^{-\bullet} \quad (8)$$

Indeed, the generalized self-exchange mechanisms in Scheme 1 contain the important earmarks of the earliest theoretical formulations of electron transfer,[4] in which the diffusive encounter (k_{diff}) of the donor/acceptor (redox) pair leads to the 1:1 precursor or encounter complex, $[\mathbf{D},\mathbf{D}^{+\bullet}]$ and $[\mathbf{A}^{-\bullet},\mathbf{A}]$, followed by the rate-limiting electron transfer (k_{ET}) to afford the successor complex $[\mathbf{D}^{+\bullet},\mathbf{D}]$ and $[\mathbf{A},\mathbf{A}^{-\bullet}]$, etc. It is thus historically noteworthy that the earliest formulation of the diffusive encounters of electron donor/acceptor pairs by Mulliken[15a] identifies the electronic transition that characterizes the various 1:1 associates as *charge transfer* to encompass the HOMO−LUMO gap. Since the related theoretical concept is involved as the *intervalence* transition in the Hush formulation,[11] their descriptions of the precursor complex must be considered interchangeable,[65] i.e., $h\nu_{IV}(\text{Hush}) = h\nu_{CT}$ (Mulliken), and the preequilibrium steps in Scheme 1 are diffusion limited, as described in (all) other electron-transfer theories. Under these circumstances, the energy of the intervalence (charge-transfer) transition within the transient complex (TC) can be directly considered in the context of the activation barrier for adiabatic electron transfer in the precursor complex (PC), in line with the classical two-state model developed by Hush for mixed-valence systems.[11,55]

3.2. Steric Effects on the Potential-Energy Surfaces for Ion-Radical Self-Exchange. Electron transfer occurring within the precursor complex plays a crucial role for the overall kinetics for Scheme 1. According to Sutin et al.,[66] the adiabatic ground-state (GS) and the excited-state (ES) energies for such a complex are obtained via the interaction of the diabatic states at each point (X) along the electron-transfer reaction coordinate as

$$E_{GS,ES} = (H_{DD} + H_{AA})/2 \pm ((H_{DD} - H_{AA})^2 + 4H_{DA}^2)^{1/2}/2 \quad (9)$$

where $H_{DD} = \lambda X^2$ and $H_{AA} = \Delta G_{ET} + \lambda(X-1)^2$ represent the energies of the initial and final diabatic states along the reaction coordinate, and the coupling element H_{DA} is assumed to be

(64) The experimental numbers in Table 5 represent the averaged values over a variety of mutual arrangements involving multiple local minima around the basic structure, as discussed in ref 22. The most common example of such a deviation is the lateral shift parallel or perpendicular to the main axis, as well as mutually perpendicular arrangements. Earlier analysis of tetrathiafulvalene dyads showed that several local maxima result from such deviations, and a somewhat similar behavior can be expected for other systems. For example, for **TMPD** the mutual arrangement atop each other (as in its salt with the ClO_4^- counterion) is characterized by $H_{DA} = 2.1 \times 10^3$ cm^{-1}, while the value of $H_{DA} = 2.6 \times 10^3$ cm^{-1} pertains to the dyad resulting from shifts by ~1.8 Å parallel to the main axis. Likewise, the crossed structure produces the rather small coupling of $H_{DA} = 0.2 \times 10^3$ cm^{-1}. In contrast, the lateral shift of dimethoxybenzene moieties leads to a decrease of H_{DA}, but in this case, the parallel and crossed structures are characterized by comparable values of H_{DA}= (2.4 and 1.7) $\times 10^3$ cm^{-1}, respectively. The energy differences among such in-plane (librational) excursions are expected to be minor in solution.[28]

(65) (a) See: Le Magueres et al. in ref 50 and references therein. (b) It should be noted that, in Mulliken theory, the charge-transfer transitions in intermolecular complexes are primarily considered in terms of the constituent donor/acceptor redox or ionization potentials, whereas, in Hush theory, the intervalence transition in localized or *bridged* (intramolecular) mixed-valence complexes are primarily related to the reorganization energies. Since the ion-radical associates of interest in this study are *intermolecular* mixed-valence complexes, we refer to the NIR optical transitions as charge transfer or intervalence interchangeably to combine both features.

(66) Brunschwig, B. S.; Sutin, N. *Coord. Chem. Rev.* **1999**, *187*, 233.

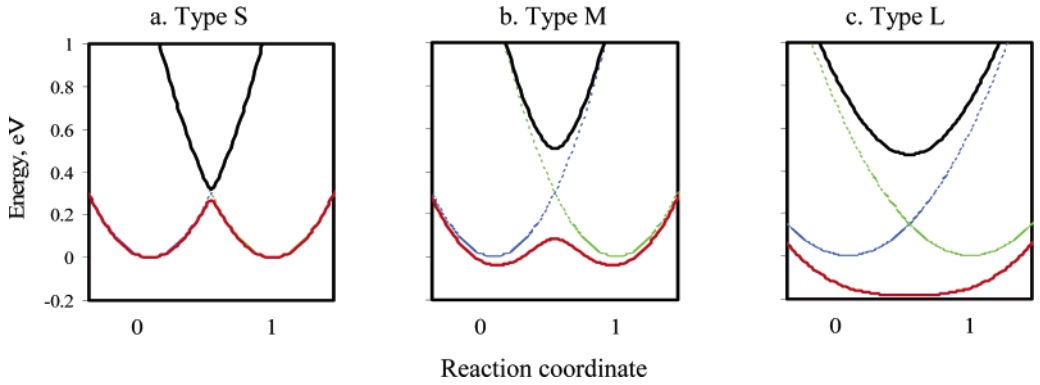

Figure 5. Representative energy diagrams for electron transfer within ion-radical complexes: (a) sterically hindered [**TPPD/TPPD**]$^{+\bullet}$ with $H_{ab} = 250$ cm^{-1} $\ll \lambda/2$; (b) sterically open [**TMPD/TMPD**]$^{+\bullet}$ with $H_{ab} = 1700$ cm^{-1} $< \lambda/2$, and (c) in the sterically close [**OMB/OMB**]$^{+\bullet}$ with $H_{ab} = 2700$ cm^{-1} $> \lambda/2$.

constant. Thus, the spectral (or computational) evaluation of the reorganization energies and coupling elements allows us to calculate the energy surface for electron transfer within various ion-radical complexes with $\Delta G^\circ = 0$. Sutin's development[12,66] of the Marcus−Hush formulation[10,11] specifically describes how the electronic coupling element (H_{DA}) directly affects the ET transition state, as illustrated in the potential-energy diagrams in Figure 5. In each case, the lightly dashed parabolic curves portray the separate reactant (blue) and product (green) diabatic surfaces, respectively, the electronic interaction of which leads to the overall potential-energy surface for electron transfer shown as the lower (heavy red) curves.

The sequence in Figure 5a−c represents typical examples of the increasing interplay between the "intrinsic" barrier (λ) and the "resonance" stabilization (H_{DA}) of the transition state. In particular, these are arbitrarily classified as three limiting energy surfaces for electron transfer, which are designated as (a) Type S with $\lambda/2 \gg H_{DA}$, (b) Type M with $\lambda/2 \geq H_{DA}$, and (c) Type L with $\lambda/2 \leq H_{DA}$. In practice, these three limiting types of the free-energy profiles as illustrated in Figure 5 are found experimentally for the **TPPD/TPPD**$^{+\bullet}$, **TMPD/TMPD**$^{+\bullet}$, and **OMB/OMB**$^{+\bullet}$ dyads in which the H_{DA} values are small (250 cm^{-1}), medial (1700^{-1}), and large (2500 cm^{-1}), respectively, in comparison to λ; and this series also reflects the decreasing trend in the steric hindrance extant between these donor/acceptor moieties (vide supra).

3.3. Electron-Transfer Mechanisms for Ion-Radical Self-Exchanges. The Mulliken−Hush delineation of the potential-energy surfaces into the three distinctive categories, Type S, M, and L, as depicted in Figure 5, necessitates the reevaluation of the generalized mechanistic proposal for self-exchange, as initially presented in Scheme 1 (eqs 7 and 8) in the following way.

3.3.1. Energy-profile Type S encompasses the precursor complex of sterically hindered ion radicals in which the interplanar separation of $r_\pi \approx 5-6$ Å is characterized by electronic coupling elements of $H_{DA} \approx 100-300$ cm^{-1}. Their adiabatic (state) energies are likely to approximate those of the diabatic states, with notable deviations being only observed at or around the transition state. No significant resonance stabilization of the ground state of the precursor complex is evident, and thus its formation constant is usually insufficient for experimental detection. It should be stressed, however, that although the coupling of ~200 cm^{-1} has only a rather minor effect on the transition energy in such a system, it is sufficient to ensure adiabatic electron transfer and the electronic transmission factor for electron transfer will be close to unity, and the second-order rate constants k_{SE} for the bimolecular electron-transfer processes in Scheme 1 can be described as

$$k_{SE} = Z \exp(-\Delta G^*/RT) \qquad (10)$$

where $Z = 10^{11}$ M^{-1} s^{-1} is the collision frequency, and the activation barrier (for $\Delta G^\circ = 0$) is[67]

$$\Delta G^* = (\lambda - 2H_{ab})^2/4\lambda \qquad (11)$$

The application of eqs 10 and 11 using the reorganization energies and coupling elements evaluated for the hindered donor/acceptor dyads in Table 5 leads to the second-order rate constants listed in Table 6 which are in reasonable agreement with the experimental values.

Table 6. Comparison of the Experimental and Calculated Rates Constants for Electron-Transfer Self-Exchange of Organic Ion Radicals[a]

ion radical		ΔG^*,[b] (kcal/mol)	k_{SE} (calcd),[c] (10^9 M^{-1} s^{-1})	k_{SE} (expt), (10^9 M^{-1} s^{-1})
1a	**OMB**$^{+\bullet}$	0	3.2	2.4
2	**OMA**$^{+\bullet}$	0	6.3	2.5
3a	**TMPD**$^{+\bullet}$	2.9	0.8	2.3
3b	**TPPD**$^{+\bullet}$	6.2[c]	0.003	0.01
4a	**PTZ**$^{+\bullet}$	1.3	7.0	4.7
4c	**PrPTZ**$^{+\bullet}$	3.2[c]	0.4	0.3
5a	**DMB**$^{+\bullet}$	2.2	1.0.	1.5
5b	**DBB**$^{+\bullet}$	3.3[c]	0.3	0.1
6	**TTF**$^{+\bullet}$[d]	0.4	7.5	2.7
7	**TCNE**$^{-\bullet}$[e]	2.2	10	4.3
8	**DDQ**$^{-\bullet}$	1.2	7.5	2.5
9	**TCNQ**$^{-\bullet}$	0.6	7.5	3.3

[a] In CH_2Cl_2 at 295 °C. [b] With eq 11. [c] See Experimental Section for calculation details. [d] Reference 22. [e] Reference 28b.

3.3.2. Energy-profile Type M is characterized by coupling elements for sterically "open" ion radicals that form mixed-valence precursor complexes with interplanar separations of $r_\pi = 3.0-3.3$ Å and the coupling elements of $H_{DA} \approx 1000-3000$ cm^{-1} which measurably alter the potential-energy surface for the electron transfer within the precursor complex, as is

(67) (a) Note that the activation barrier and the calculated electron-transfer rates are affected even by such relatively small values of H_{DA}. For example, in the *p*-phenylenediamine system with $\lambda = 9500$ cm^{-1}, the correction for $H_{ab} = 250$ cm^{-1} leads to a 3-fold increase in rate. (b) We believe that, in Type S systems, the electronic coupling between redox centers in organic donor/acceptor dyads is sufficient for adiabatic electron transfer even for the sterically hindered moieties. Compare: Nelsen, S. F.; Pladziewicz, J. R. *Acc. Chem. Res.* **2002**, *35*, 247.

characteristic of Robin−Day Class II mixed-valence systems.[56] Thus, even for dyads with relatively low ratios of H_{DA}/λ, such as **TMPD**$^{+\bullet}$**/TMPD**, the barrier for electron transfer is roughly halved relative to those in weakly interacting systems with $\Delta G^* = \lambda/4$. Moreover, the ground-state stabilization of such a system enables this precursor complex to be observed in solution with the aid of electronic (NIR) spectroscopy and its formation constant to be calculated generally in the order of $K_\pi \approx 0.1-1$ M^{-1} in Table 3. It is also possible to calculate the overall rate of the self-exchange process for the energy profile based on the experimentally measured formation constant (K_π) of the ion-radical complex and the intramolecular rate constant (k_{ET}) given as[68]

$$k_{ET} = \kappa_{el}\nu_n \exp(-\Delta G^*/RT) \qquad (12)$$

Notably, the $k_{ET}K_\pi$ product for the "open" ion radicals described in Table 1 (with the formation constant of the precursor complex taken from Table 3) is close to, or even faster than, the bimolecular diffusion rate, as evaluated by $k_{diff} = 1.5 \times 10^{10}$ M^{-1} s^{-1} in CH_2Cl_2 at 295 K. Therefore, the self-exchange rate constant k_{SE} for the bimolecular electron-transfer process in Scheme 1 must be recalculated from the standard steady-state approximation,[69] i.e.,

$$1/k_{SE}^{calcd} = 2/k_{diff} + 1/K_\pi k_{ET} \qquad (13)$$

and these values of the second-order rate constant for the self-exchange are included in Table 6.

Strongly coupled Class II complexes (such as those involving **TTF**),[22] with large ratios of H_{DA}/λ, are characterized by higher equilibrium constants in the range of $K_\pi \approx 1-10$ M^{-1}. Most importantly, the barriers for electron transfer within such ion-radical complexes drop to almost zero, and they consequently approach the Robin−Day Class II/Class III borderline. On the other hand, such dyads as (**DDQ**)$_2^{-\bullet}$ and (**TCNQ**)$_2^{-\bullet}$ show equilibrium constants in the same range, but the solvent dependence of their NIR bands reveals their possible delocalized nature. It thus appears that these precursor complexes also lie close to the Class III/Class II border but more on the delocalized side.

3.3.3. Energy-profile Type L includes ion-radical complexes that lie beyond the Class II/III border. Owing to the large values of H_{DA} (relative to λ) resulting in the complete delocalization of the electron in the Robin−Day Class III (ion-radical) associates,[71] the separate precursor and successor complexes in the electron-transfer mechanism in Scheme 1 must be replaced by a single intermediate as shown in Scheme 2. Thus, the overall

Scheme 2

$$\mathbf{D} + \mathbf{D}^{+\bullet} \rightleftharpoons [\mathbf{D},\mathbf{D}]^{+\bullet} \rightleftharpoons \mathbf{D}^{+\bullet} + \mathbf{D} \qquad (14)$$

self-exchange processes according to Scheme 2 are controlled by (diffusive) association and dissociation of the π-complexes. Notably, the experimental characteristics of the delocalized complex near or beyond the Class II/III border are generally similar to those of strongly coupled Class II systems. However, the increased stability of an ion-radical complex such as **OMB**/**OMB**$^{+\bullet}$ (which is characterized by the formation constant of $K_\pi \approx 350$ M^{-1}) results in the appearance of principal new features. First, such high equilibrium constants from the kinetics point of view necessitates the rate constant for dissociation to be explicitly taken into account, since dissociation can become the rate-limiting step. Indeed, numerical calculations of the self-exchange (see Experimental Section for details) result in rate constants for self-exchange of **OMB** which are slower than those determined for Robin−Day Class II systems discussed above. Moreover, lowering the temperature can result in decreased rates of (**OMB**)$_2^{+\bullet}$ dissociation. Thus, the exchange rates between the monomeric and dimeric paramagnetic species can even become slow on the EPR time scale, such that two separate EPR spectra can be simultaneously observed. At very low temperatures, almost all the monomer is associated, and the pure spectrum of the dimeric (**OMB**)$_2^{+\bullet}$ with a doubled number of lines and halved splitting constants is observed in solutions containing both **OMB**$^{+\bullet}$ and **OMB**.[70] Moreover, the high equilibrium constants for such a π-complex formation is further reflected in the unusual electrochemical behavior of **OMB** that shows the oxidation wave to be split upon lowering the temperature. Although quantitative modeling of the splitting is beyond the scope of the current work, qualitatively it is related to the fast (and significant) complex formation of the oxidized species while the neutral donor is still available in solution at the earliest stages (i.e., foot) of the CV wave. Indeed, the anodic behavior of the dimeric (**OMB**)$_2^{+\bullet}$ is similar to the splitting of the oxidation wave previously observed in mixed-valence (bridged) systems.[8b]

3.4. Conciliation of Organic versus Inorganic Electron-Transfer Mechanisms. The foregoing comprehensive description of organic electron-transfers contains a number of important features in common with Taube's seminal dichotomy into separate outer-sphere and inner-sphere electron-transfer mechanisms based on the behavior of inorganic coordination complexes, as follows in (i), (ii), and (iii) below.

(i) The outer-sphere versus the Type S process for self-exchange lie co-incident at one end of a mechanistic spectrum since both of their loosely bound (degenerate) precursor and successor complexes exhibit only weak electronic coupling with $H_{DA} < 200$ cm^{-1} characteristic for electron-transfer processes of inorganic redox dyads which are adequately described by Marcus (outer-sphere) theory.[10]

(ii) At the other mechanistic extremum, the classical (Taube) inner-sphere mechanism and the Type L pathway both occupy the other, strongly adiabatic limit in which the extensive electronic couplings between donor/acceptor moieties with $H_{DA} \geq 2700$ cm^{-1} are enforced by direct ligand bridging and by intimate (cofacial) juxtapositions, respectively.[71]

If such mechanistic concepts of electron transfer are to have any generality, they must equally accommodate the complete spectrum of quantitative reactivities (including Type M) of both organic and inorganic donors and acceptors, despite any intrinsic structural differences among them.[72] Accordingly, let us proceed by extending Taube's outer-sphere/inner-sphere terminology to organic redox dyads. Since organic donors and acceptors are

(68) Where κ_{el} is the electronic transmission coefficient ($\kappa_{el} \approx 1$ for adiabatic reaction) and ν_n is the nuclear vibration frequency.[12, 66]
(69) Newton, M.; Sutin, N. *Ann. Rev. Phys. Chem.* **1986**, *35*, 435.
(70) As such, the study of **OMB** provides the direct link between the earlier separate ESR studies of the self-exchange process, on one hand, and the electronic structure of the paramagnetic dimers, on the other hand.
(71) (a) For other examples of the unusual Type L potential-energy surfaces in intermolecular electron-transfer processes, see: (b) Rosokha, S. V.; Kochi, J. K. *New J. Chem.* **2002**, *26*, 851. (c) Rosokha, S. V.; Dibrov, S. M.; Rosokha, T. Y.; Kochi, J. K. *Photochem. Photobiol. Sci.* **2006**, *5*, 914. (d) See also ref 29.

not usually considered in terms of ligand-dependent "coordination spheres", we propose an alternative allusion to "distance-dependence" which is based on the effective van der Waals radii of electron donors and acceptors.[53] In this way, the bimolecular interactions in outer-sphere processes are also viewed as those that extend beyond their van der Waals separation, as denoted by r_{OS} in Chart 1. Equivalently, the inner-sphere interactions are then those that are manifested in a measurable van der Waals' distortion owing to the close juxtaposition of donor/acceptor dyads in the precursor complex, so that the inner-sphere separation (r_{IS}) in Chart 1 is substantially more intimate than the outer-sphere separation (r_{OS}).[73]

(iii) The medial Type M potential-energy surface, on this basis, derives from the attractive electronic coupling (H_{DA}) that is sufficient to contract the donor/acceptor separation, with the magnitude of r_{IS} diagnostic of a *localized* (Class II) inner-sphere precursor complex. Likewise, the Type L potential-energy surface from a strongly coupled donor/acceptor dyad is described as a *delocalized* (Class III) inner-sphere precursor complex.[71]

It is important to note that for both Type M and L systems the spectroscopic observations of the intermolecular charge-transfer or intervalence absorption bands are the experimental harbinger of the inner-sphere interactions extant within the precursor complexes because such HOMO → LUMO transitions are absent (or very weak) when the donor/acceptor separations lie beyond the van der Waals limit.[53]

4. Summary and Conclusions

The three limiting potential-energy surfaces described in Figure 5 as Types S, M, and L, in a more general mechanistic context, can be represented as an alternative, expanded version of Taube's seminal dichotomy into separate outer-sphere and inner-sphere electron-transfer transition states. First, the outer-sphere and Type S processes both occupy one end of a mechanistic spectrum (Scheme 1) that pertains to nonadiabatic or weakly adiabatic electronic transitions within the precursor complex. Second, Type M processes represent a broad intermediate range of inner-sphere mechanisms in which the intermolecular separation ($r_{DA} = r_{IS}$) between donor and acceptor moieties is considerably contracted, lying closer than the sum of their van der Waals radii, to form localized precursor complexes which are alternatively described as belonging to Robin−Day Class II. These transient donor/acceptor associates are sufficiently bound to reveal intervalence electronic transitions in which Mulliken−Hush analysis leads to the reduced reorganizational barriers by the amount: $\lambda/4 - H_{DA}$.[74] Third, the Type L process and the delocalized inner-sphere mechanism both occupy the other, strongly adiabatic limit sufficient to effect a complete donor/acceptor delocalization diagnostic of Robin−Day Class III. In this case, the separate precursor and successor complexes are merged (Scheme 2) because the intermolecular electron transfer accompanies the diffusive encounter of the donor/acceptor dyad without any reorganization barrier.

4.1. Continuum of Outer-Sphere and Inner-Sphere Mechanisms for Ion-Radical Self-Exchanges. When viewed in this way, there will be a continuous progression of precursor complexes in which the electronic coupling element (H_{DA}) is strongly and easily modulated by the donor/acceptor separation (r_{DA}) and orientation, as affected by steric factors, solvation, etc. This mechanistic picture is strongly dependent on the Mulliken−Hush formulation of the diffusive intermolecular intermediates, in which H_{DA} values can continuously vary over a range of donor/acceptor (redox) functionalities and (steric) separations.

We believe that organic donors and acceptors are ideally suited for quantitative studies of electron-transfer mechanisms for several important reasons. Thus, organic redox groups such as benzenoid and other aromatic systems as well as mono- and polyolefinic centers are planar and offer open π-access which is at the same time easily controlled, i.e., "tuned", by remote substitutents. Next, such electron donors and acceptors are, by and large, substitution stable, and the complication and ambiguity from extraneous pre-equilibrium processes can be circumvented. Most important, the electronic transitions that characterize the critical precursor complex can usually be found in accessible spectral regions for experimental (Mulliken−Hush) and theoretical analysis.

Finally, we hope that the "separation-based" measure of the precursor complex ($r_{DA} = r_{OS}$ or r_{IS}) will provide useful and quantitative insights for the mechanistic evaluation of a variety of other electron-transfer processes, especially as they apply to hybrid organic/inorganic,[15] metalloorganic,[13c] and biochemical[17] redox dyads of increasing relevance in today's diversified applications.

5. Experimental Section

5.1. Materials. Tetramethyl-*p*-phenylenediamine (**TMPD**), phenothiazine (**PTZ**), *N*-methylphenothiazine (Me**PTZ**), tetrathiafulvalene, (**TTF**), dichlorodicyanobenzoquinone (**DDQ**), tetracyanoethylene (**TCNE**), and tetracyanoquinodimethane (**TCNQ**) from commercial sources were purified by sublimation in vacuo and/or by recrystallyzation. Octamethylbiphenylene (**OMB**),[41a] octamethylanthracene (**OMA**),[41a] tetra-isopropyl-*p*-phenylenediamine (**TPPD**),[41b] and dimethoxydimethylbenzene (**DMB**)[72f] were synthesized and identified according to the literature procedures. Solvents were prepared and handled as described earlier.[23b] Cation-radical salts $\mathbf{D}^{+\bullet}CB^-$ and $\mathbf{D}^{+\bullet}SbCl_6^-$ were produced in dichloromethane by oxidation of the donor with stoichiometric (1:1) amounts of either dodecamethylcarboranyl radical $CB^\bullet$ (prepared by oxidation of Cs^+CB^- with PbO_2)[34] or nitrosonium salt $NO^+SbCl_6^-$[35] and precipitated with hexane. Anion-radical salts K^+(cryptand) $\mathbf{A}^{-\bullet}$ were prepared either by potassium-mirror reduction of the corresponding electron acceptor in THF in the presence of a stoichiometric amount of [2,2,2]cryptand[31] or by addition of stoichiometric amounts of the cryptand to the suspension of the potassium salt: $K^+\mathbf{A}^{-\bullet}$ in dichloromethane. The mixture was stirred until dissolution was complete which was then followed by precipitation with hexane. Colorless single crystals of the hindered donors (**DBB**, **PrPTZ**) were prepared by the slow evaporation of their solution in dichloromethane at room temperature. To prepare single crystals of the cation-radicals salts, $\mathbf{TPPD}^{+\bullet}SbCl_6^-$, $\mathbf{DBB}^{+\bullet}CB^-$, $\mathbf{DMB}^{+\bullet}CB^-$, $\mathbf{PTZ}^{+\bullet}CB^-$, $\mathbf{PrPTZ}^{+\bullet}CB^-$,

(72) For example, inorganic donor/acceptor dyads are metallocentric, and electron transfer is largely directed between single atomic centers. In contrast, organic donor/acceptor dyads involve multiple (carbon) centers, and electron transfer is consequently more diffusive. Moreover, ligands usually play important roles in inorganic (coordination) donors and acceptors, whereas the concept is alien to and essentially undefined in organic donors and acceptors.

(73) (a) Under these circumstances, the molecular or atom-bridged activated complex of Taube can be approximated as either a type M or L system in which the bridged is considered virtual, as in the case of a mixed organic/inorganic (distorted) redox dyad. See: (b) Fukuzumi, S., et al. in ref 33b. (c) Kochi, J. K. *Pure Appl. Chem.* **1990**, *52*, 571. See also: (d) Kochi, J. K. in ref 13c. (e) For the quantitative comparison of the electronic coupling in the intramolecular (bridged) mixed-valence system relative to that in the corresponding intermolecular cofacial (through-space) system, see: (f) Sun, D. L.; Rosokha, S. V.; Lindeman, S. V.; Kochi, J. K. *J. Am. Chem. Soc.* **2003**, *125*, 15950. Sun et al. in ref 23b.

(74) Marcus, R. A. *J. Phys. Chem.* **1992**, *96*, 1753.

the salts were dissolved in dichloromethane, and the solutions were overlaid with hexane at room temperature. The mixture was then slowly cooled to −60 °C and kept at this temperature for several days. To prepare single crystals of the $(\mathbf{DDQ})_2^{-\bullet}$ complex, equimolar amounts of the parent acceptor (**DDQ**) was added to the clear solution obtained by the addition of 15-crown-5 polyether ligand (in 2:1 molar ratio) to the suspension of the potassium salts $K^+\mathbf{DDQ}^{-\bullet}$. The solution was then covered with hexane, cooled to −60 °C, and kept at this temperature for several weeks. This resulted in the formation of dark brown crystals of the (1:1) anionic π-complex as the bis-ligated potassium salt: $K(15\text{-crown-}5)_2^+$ $(\mathbf{DDQ})_2^{-\bullet}(\mathbf{DDQ})$.

5.2. X-ray Crystallography. The intensity data for the X-ray studies were collected at −100 °C with a Bruker SMART Apex diffractometer equipped with a CCD detector using Mo Kα radiation (λ = 0.710 73 Å). The structures were solved by direct methods and refined by a full matrix least-squares procedure as described earlier.[75] The crystallographic data are presented in Table S1 in the Supporting Information.

5.3. Electrochemistry. Cyclic voltammetry (CV) and Osteryoung square-wave voltammetry (OSWV) were performed on a BAS 100A Electrochemical Analyzer in dichloromethane with n-$Bu_4N^+PF_6^-$ as the supporting electrolyte, and ferrocenium salt with $E°$ = 0.475 V vs SCE was added as the internal standard, as described previously.[23]

5.4. Spectral (UV−vis−NIR) Measurements. Electronic absorption spectra were recorded on a Varian Cary 5 spectrometer in Teflon-capped quartz cuvettes. Formation of the dimeric $(\mathbf{D})_2^{+\bullet}$ and $(\mathbf{A})_2^{-\bullet}$ was studied under an argon atmosphere at room temperature (22 °C) in dichloromethane. The measurement of the new NIR bands (in the 1000−3000 nm range) was effected when the donor was added to the solution of its cation radical or the acceptor was added to the solution of its anion radical. The quantitative analysis of the intensities of the NIR absorption bands with the aid of Benesi−Hildebrand or Drago procedures as described earlier[23a] afforded the formation constants (K_π) and extinction coefficients (ϵ_π) of the 1:1 complexes. Since these procedures were approximate, the K_π and ϵ_π values were also evaluated more precisely by the computer fitting (by K_π and ϵ variations) of the experimental absorptions (measured in series of solutions with different concentrations of the donor or the acceptor and their ion-cation radical salts). The exact expression $A = 0.5 \times \epsilon \times \{(D_0 + D_0^+ + 1/K_\pi) - [(D_0 + D_0^+ + 1/K_\pi)^2 - 4 \times D_0 \times D_0^+]^{0.5}\}$ was employed, where D_0 and D_0^+ were the concentrations of the donor and the cation-radical salt added. The same procedure was applied to the solutions of the electron acceptors and their anion-radical salt. Subsequent measurements of K_π at different temperatures with the aid of a Dewar equipped with quartz windows resulted in the enthalpy and entropy changes ΔH_π and ΔS_π for the formation of the π-complex.

5.5. EPR measurements were performed on a Bruker ESP-300 X-band spectrometer, and the hyperfine splitting constants were determined by computer simulation of the ESR spectra of pure anion-radical salts using the WinSim program.[76] Kinetic parameters for intermolecular electron-transfer self-exchange were determined from the (general) line broadening of ion-radical spectra in the presence of added (neutral) donor or acceptor.[43] The self-exchange processes with the $\mathbf{PTZ}^{+\bullet}$ and $\mathbf{TMPD}^{+\bullet}$ cation radicals were measured in dichloromethane in the fast exchange limit, and their second-order rate constants were calculated as $k_{SE} = 2.05 \times 10^7 \times \nabla/(\Delta\Delta H/\Delta C)$, where $\Delta\Delta H/\Delta C$ represented the slope of the width of a single line in the EPR spectrum on the concentration of added neutral donor or acceptor, and the ∇ is the second moment of the EPR spectra. With the other ion radicals, the measurements were carried out in the slow exchange limit (since the solubilities of the parent donors and acceptors in dichloromethane were not sufficient to satisfy the criteria for the measurements in the fast exchange limit, i.e., $(3/4\Delta)^{1/2}\Delta\Delta H < 0.2$). Accordingly, the second-order rate constants for the sterically open ion-radicals $\mathbf{OMB}^{+\bullet}$, $\mathbf{OMA}^{+\bullet}$, $\mathbf{DMB}^{+\bullet}$, $\mathbf{DDQ}^{-\bullet}$, $\mathbf{TCNQ}^{-\bullet}$ (which were characterized by relatively simple EPR spectra) were calculated as $k_{SE} = 1.52 \times 10^7 \times \Delta\Delta H/\Delta C/(1 - P_i)$, where $\Delta\Delta H/\Delta C$ represented the slope of the width of the central line in the EPR spectrum on the concentration of added neutral donor or acceptor, and $(1 - P_i)$ is exchange-probability correction. For the sterically hindered cation-radicals $\mathbf{TPPD}^{+\bullet}$, $\mathbf{DBB}^{+\bullet}$, and $\mathbf{PrPTZ}^{+\bullet}$ (which are characterized by complex EPR spectra), the line width variation with concentration of added donor were evaluated via the EPR spectra simulations with the WINSIM program.[76] The self-exchange rate constants k_{SE}(calcd) in Table 6 for the $\mathbf{TMPD}^{+\bullet}$, $\mathbf{PTZ}^{+\bullet}$, $\mathbf{DMB}^{+\bullet}$, $\mathbf{DDQ}^{-\bullet}$, and $\mathbf{TCNQ}^{-\bullet}$ were calculated via eq 13 with K_π taken from Table 3; the first-order rate constant k_{ET} calculated according to eq 12 (with a preexponential factor of 10^{12} s^{-1}, as discussed earlier[23]). For the sterically hindered $\mathbf{TPPD}^{+\bullet}$, $\mathbf{PrPTZ}^{+\bullet}$, and $\mathbf{DBB}^{+\bullet}$, the rate constants were calculated via eq 10 since experimental values of K_π were not available. In these cases, the activation barriers were calculated using H_{DA} = 200 cm^{-1} (as discussed in text) and the reorganization energy was taken from the unhindered (open) analogues. For $\mathbf{OMB}^{+\bullet}$ and $\mathbf{OMA}^{+\bullet}$, the rate constants were calculated by the numerical solution (with Mathematica program) of the system of differential equations describing the process in eq 14, as described earlier.[28b] In these calculations, the rate constants for complex formation were taken as being equal to the diffusion rate constant, and the rate constants of the complex dissociation were calculated as $k_{diss} = k_{diff}/K_\pi$.

5.6. Computational Methodologies. The reorganization energy for the electron transfer within the complexes was calculated as a sum of the inner- and outer-sphere components. The intramolecular contribution (λ_i) to the overall reorganization energy for electron transfer within paramagnetic ion-radical dyads was calculated as the difference between the initial diabatic state (with the electron located on the donor (**D** or $\mathbf{A}^{-\bullet}$) with reactants in their relaxed geometries) and the final diabatic state (with the same nuclear geometry but the electron transferred to the acceptor ($\mathbf{D}^{+\bullet}$ or **A**)).[57] For example, in the case of cation-radical complexes, $\lambda_i^{calcd} = \{E_c(r_n) + E_n(r_c)\} - \{E_n(r_n) + E_c(r_c)\}$, where r_n and r_c are the optimized coordinates and E_n and E_c are the energies of the neutral donor and its cationic counterpart. Accordingly, we first optimized the geometry of the donor and the corresponding cation radicals and determined their energies, $E_n(r_n)$ and $E_c(r_c)$ via Hartree−Fock and DFT computations with the aid of Gaussian 98 (6-311G* basis and B3LYP functional).[77] Then the single-point calculation of $\mathbf{D}^{+\bullet}$ in the geometry of the neutral **D** led to $E_c(r_n)$, and the neutral donor in the geometry of the cation produced the values of $E_n(r_c)$. The energy differences afforded the inner-sphere reorganization energies, listed in Table S4 which also contains computational details as well as values calculated via an analogous procedure for anion-radical complexes.

For calculations of the solvent reorganization energy, the ion-radical π-complex was considered as a cavity of radii a_0 with an internal dielectric constant of ϵ_{in} = 2 immersed in a solvent with static and optical dielectric constants ϵ_s = 8.93 and ϵ_o = 2.028.[43c] The reorganization energy λ_o^{calcd} based on the Kirkwood solvation model is given by[28,58]

$$\lambda_o^{calcd} = {}^1/_2 a_0(1/\epsilon_{in} - 1/\epsilon_s)\sum_n g_n/(1 + [n/(n+1)]\epsilon_{in}/\epsilon_s) - (1/\epsilon_{in} - 1/\epsilon_0)\sum_n g_n/(1 + [n/(n+1)]\epsilon_{in}/\epsilon_0)$$

where

$$g_n = \sum\sum_{k,j} \Delta e_k \Delta e_j (r_k/a_0)^n (r_j/a_0)^n P_n(\cos\theta_{j,k}), \text{ with } n = 1 \text{ to } 6$$

(75) (a) Sheldrick, G. M. *SADABS* (ver. 2.03); 2000. (b) Sheldrick, G. M. *SHELXS 97*; University of Göttingen: Germany, 1997.
(76) Duling, D. *PEST WinSim*, version 0.96. Public EPR Software Tools, National Institute of Environmental Health Sciences: 1996.
(77) Pople, J. A., et al. *Gaussian 98*, revision A.11.3 ed.; Gaussian, Inc.: Pittsburgh, PA, 2001.

Δe_j denotes the variation of the charge on the jth atom, N is the number of atoms, r_j locates the jth atom in space, $\theta_{j,k}$ is the angle between r_j and r_k, and P_n are ordinary Legendre functions. The atomic coordinates in the complexs were taken from their X-ray structures (if unavailable, those the from related diamagnetic dimers $(\mathbf{D})_2^{2+}$ or $(\mathbf{A})_2^{2-}$], and values of a_0 were calculated from the molecular volume of such dyads (from the single-point Gaussian 98 computation) plus 0.5 Å.[77] The atomic charges for the ion-radical π-complex in the hypothetical diabatic state were taken via the Gaussian 98 computation of the isolated neutral donors and acceptors and their ion radicals (ESP charges, CHELPG option).[77]

The ab initio evaluation of the electronic coupling elements (H_{DA}) in Table 5 between symmetry-equivalent donor/acceptor moieties was carried out as described earlier.[28,59] This was based on the single-point Hartree−Fock and/or B3LYP Gaussian-98 computations (with 6-311G* basis set) of the energy splitting resulting from the symmetric and antisymmetric combinations of the localized molecular orbitals of the monomers within the neutral closed-shell dimeric species. In particular, for the cationic mixed-valence complexes, the coupling elements were calculated as one-half of the difference between the HOMO and HOMO − 1 (highest-lying alpha occupied eigenvalues) obtained using the Pop = Regular option in the single-point Gaussian computations of the corresponding neutral dimers. The atomic coordinates of the dyad were taken from the X-ray structures of the appropriate cationic or dicationic dimers (see Table S4 in the Supporting Information) but with additional electrons to generate neutral closed-shell systems. Likewise for the anionic mixed-valence complexes, the coupling elements were calculated as one-half of the energy difference between the LUMO + 1 and LUMO (lowest-lying alpha virtual eigenvalues) computed for the corresponding neutral closed-shell dyads.[60] The dimeric species were based on the geometries of the anionic or dianionic dimers but with one or two fewer electrons. For example, to calculate H_{DA} for the $(\mathbf{DDQ})_2^{-\bullet}$ complex, we extracted the atomic coordinates of the centrosymmetric mixed-valence dimeric unit from the X-ray structure of K(15-crown-5)$_2^+$(**DDQ**)$_2^{-\bullet}$(**DDQ**) (vide supra). With these coordinates, we carried out the single-point Gaussian computations of the neutral $(\mathbf{DDQ})_2$ dimer with the Pop = Regular option to produce the orbital energies. Finally, the coupling element was calculated as $H_{DA} = {}^1/_2[E(\text{LUMO} + 1) - E(\text{LUMO})]$, where the energies of LUMO and LUMO + 1 were taken as the lowest-lying alpha virtual eigenvalues. For the calculations of the dependence of H_{DA} values on the interplanar separation in Figure 4, the atomic coordinates were generated by artificially increasing the interplanar separation in the experimental X-ray structure. For the calculation of H_{DA} values of the complexes with crossed monomer moieties, the atomic coordinates were generated by rotating one of the monomeric units in the experimental X-ray structure by 90°.

Acknowledgment. We thank J. M. Lu for the synthesis of **PrPTZ** and the preparation of the single crystal, as well as the preparation and the spectral (UV−NIR, ESR) measurements of the $\mathbf{D}^+SbCl_6^-$ salts; T. Y Rosokha for the preparation of the single crystals of **TPPD**$^{+\bullet}SbCl_6^-$, **DMB**$^{+\bullet}CB^-$, **PrPTZ**$^{+\bullet}CB^-$, and **PTZ**$^{+\bullet}CB^-$, and K(15-crown-5)$_2^+$(**DDQ**)$_2^{-\bullet}$(**DDQ**); A. S. Jalilov for the synthesis of **DBB**, **DBB**$^{+\bullet}CB^-$ and the preparation of the single crystals, as well as for electrochemical measurements; D. Sun for the synthesis of **TPPD**; B. Han for ESR measurements of the **DDQ**$^{-\bullet}$ anion radical; I. S. Neretin for the X-ray crystallographic analysis of K(15-crown-5)$_2^+$(**DDQ**)$_2^{-\bullet}$(**DDQ**), **PrPTZ**, and **PTZ**$^{+\bullet}CB^-$; S. M. Dibrov for the X-ray analysis of **TPPD**$^{+\bullet}SbCl_6^-$, **PrPTZ**$^{+\bullet}CB^-$; and J.-J. Lu for the X-ray analysis of **DBB**, **DBB**$^{+\bullet}CB^-$, **DMB**$^{+\bullet}CB^-$ and crystallographic assistance. We thank M. D. Newton for many helpful discussions with regard to the computations of the reorganization energies and electronic coupling elements and the R. A. Welch Foundation and the National Science Foundation for financial support.

Supporting Information Available: The crystallographic data (Table S1), the charge analysis in K(15-crown-5)$_2^+$(**DDQ**)$_2^{-\bullet}$(**DDQ**) (Table S2), computations of reorganization energy (Table S3) and coupling element (Table S4), temperature-dependent voltammograms of the **OMA** (Figure S1), ESR line broadening of **DDQ**$^{-\bullet}$ upon addition of parent **DDQ** (Figure S2), NIR spectral changes showing the formation of the [**TMPD**$^{+\bullet}$, **TMPD**] complex (Figure S3); temperature dependence of the NIR spectrum of [**TCNQ**$^{-\bullet}$, **TCNQ**] (Figure S4); complete ref 77. This material is available free of charge via the Internet at http://pubs.acs.org.

JA069149M